Lecture Notes for MVComp 1

in Winter Semester 2019/2020

Fundamentals of Simulation Methods

originally by Volker Springel (MPA)

modified and extended by Cornelis Dullemond (ZAH),
Philipp Girichidis (AIP), Frauke Gräter (HITS),
Rüdiger Pakmor (MPA), Christoph Pfrommer (AIP),
Friedrich Röpke (HITS/ZAH), and Ralf Klessen (ZAH)

January 19, 2021

MPA:
Max-Planck-Institut für Astrophysik (MPA)
Karl-Schwarzschild-Str. 1
85748 Garching

ZAH:
Zentrum für Astronomie der Universität Heidelberg
Institut für Theoretische Astrophysik
Albert Ueberle Str. 2
69120 Heidelberg

HITS:
Heidelberg Institute for Theoretical Studies
Schloss-Wolfsbrunnenweg 35
69118 Heidelberg

AIP:
Leibniz-Institut für Astrophysik Potsdam
An der Sternwarte 16
14482 Potsdam

Contents

10 Basic gas dynamics

Gravity is the dominant driver behind cosmic structure formation (e.g. Mo et al., 2010), but at small scales hydrodynamics in the baryonic component becomes critical for understanding physical processes that govern e.g., the formation of galaxies. In this section we review the basic equations and some prominent phenomena related to gas dynamics in order to make the discussion of the numerical fluid solvers used in galaxy evolution more accessible. For a more detailed introduction to hydrodynamics, the reader is referred to the standard textbooks on this subject (e.g. Landau & Lifshitz, 1959; Shu, 1992).

10.1 Basic conservation equations

10.1.1 Preliminaries

A physical system can be described at different levels: with quantum physics, at the classical particle level, or in the continuous fluid level. A fluid is a macroscopic description of a physical system that is characterized by its mass density ρ, temperature T, and velocity $\boldsymbol{u} = \boldsymbol{v} + \boldsymbol{w}$. Here $\boldsymbol{v} \equiv \langle \boldsymbol{u} \rangle$ is the mean velocity in the local fluid element and $\boldsymbol{w}$ is the random velocity component that defines the temperature. The equipartition theorem of classical mechanics states that each degree of freedom i that can be excited has energy $k_{\mathrm{B}}T/2$:

$$\left\langle \frac{1}{2} m w_i^2 \right\rangle = \frac{1}{2} k_{\mathrm{B}} T \implies \left\langle |\boldsymbol{w}|^2 \right\rangle = \frac{3 k_{\mathrm{B}} T}{m}. \tag{10.1}$$

Fluid elements move and change their density and temperature, but particles random walk from one fluid element to another only slowly, through a diffusion process.

A system can be well described as a fluid, if the particle mean free path is much shorter than the characteristic system size, $\lambda \ll L$. In an ionized plasma, the electron's effective interaction radius r_{e} is to order of magnitude give by an energy balance between the electrostatic potential of an ion of charge Ze and the thermal energy of an electron:

$$\frac{Ze^2}{r_{\mathrm{e}}} \sim m_{\mathrm{e}} w_{\mathrm{e}}^2 \sim k_{\mathrm{B}} T_{\mathrm{e}}, \tag{10.2}$$

where e and m_e are the electron charge and mass, respectively. The electron mean free path is given by

$$\lambda = \frac{1}{n\sigma} \sim \frac{1}{n\pi r_\mathrm{e}^2} \sim \frac{1}{\pi n}\left(\frac{k_\mathrm{B}T_\mathrm{e}}{Ze^2}\right)^2 \tag{10.3}$$

$$\sim 1.5\times10^{22}\left(\frac{n}{10^{-3}\ \mathrm{cm}^{-3}}\right)^{-1}\left(\frac{k_\mathrm{B}T_\mathrm{e}}{1\ \mathrm{keV}}\right)^2\ \mathrm{cm}, \tag{10.4}$$

where we have assumed $Z = 1$ and scaled the values to typical conditions of the intracluster medium.

Careful calculations (analogous to those performed in Chapter **??** in the context of a collisionless gravitating system) yield a result that is shorter by the Coulomb logarithm ($\sim (\ln\Lambda)^{-1}$) because of the effects of distant interactions. Here, $\Lambda = b_\mathrm{max}/b_\mathrm{min}$ is the ratio of the largest-to-smallest impact parameter of such an interaction. The typical impact parameter in a large-angle deflection constitutes the minimum impact parameter, $b_\mathrm{min} \sim r_\mathrm{e}$, and $b_\mathrm{max} \sim \lambda_\mathrm{D}$ since the plasma becomes neutral on scales larger than the Debye length, $\lambda_\mathrm{D} = \sqrt{k_\mathrm{B}T/(4\pi n_\mathrm{e}Ze^2)}$. Hence, we obtain to order of magnitude

$$\ln\Lambda \sim \ln\frac{\lambda_\mathrm{D}}{r_\mathrm{e}} \sim \ln\sqrt{\frac{(k_\mathrm{B}T)^3}{n_\mathrm{e}4\pi Z^3e^6}}$$

$$\sim 35 - \frac{1}{2}\ln\left(\frac{n_\mathrm{e}}{10^{-2}\mathrm{cm}^{-3}}\right) + \frac{3}{2}\ln\left(\frac{k_\mathrm{B}T}{\mathrm{keV}}\right). \tag{10.5}$$

Hence, $\lambda \ll L_\mathrm{cluster}$ and we can treat the bulk of the intracluster medium as a fluid. However, on small scales or toward the cluster outskirts, this is not true and we have to consider plasma processes.

10.1.2 The distribution function and the Boltzmann equation

We define the distribution function $f(\boldsymbol{x}, \boldsymbol{u}, t)$ such that $f(\boldsymbol{x}, \boldsymbol{u}, t)\mathrm{d}^3x\mathrm{d}^3u$ is the probability of finding a particle in the phase space volume $\mathrm{d}^3x\mathrm{d}^3u$ centered on position $\boldsymbol{x}$, velocity $\boldsymbol{u}$ at time t. Integrating over all phase space yields the total number of particles

$$N = \int\int f(\boldsymbol{x}, \boldsymbol{u}, t)\mathrm{d}^3x\mathrm{d}^3u. \tag{10.6}$$

Since particles are neither created nor destroyed, continuity implies

$$\frac{\mathrm{d}}{\mathrm{d}t}f(\boldsymbol{x}, \boldsymbol{u}, t) = \frac{\partial f}{\partial t} + \dot{\boldsymbol{x}}\cdot\boldsymbol{\nabla}f + \dot{\boldsymbol{u}}\cdot\boldsymbol{\nabla}_u f = \left.\frac{\mathrm{d}f}{\mathrm{d}t}\right|_\mathrm{c}, \tag{10.7}$$

where the term $\mathrm{d}f/\mathrm{d}t|_\mathrm{c}$ represents discontinuous motions of particles through phase space as a result of collisions. While collisions happen at a fixed point in space, they

can instantaneously change particle velocities and thus cause particles to jump in phase space. Substitution $\dot{\boldsymbol{x}} = \boldsymbol{u}$ and $\dot{\boldsymbol{u}} = \boldsymbol{g}$ leads to the Boltzmann equation

$$\frac{\mathrm{d}}{\mathrm{d}t} f(\boldsymbol{x}, \boldsymbol{u}, t) = \frac{\partial f}{\partial t} + \boldsymbol{u} \cdot \boldsymbol{\nabla} f + \boldsymbol{g} \cdot \boldsymbol{\nabla}_u f = \left.\frac{\mathrm{d}f}{\mathrm{d}t}\right|_{\mathrm{c}} \tag{10.8}$$

which describes the evolution of the phase space distribution function $f(\boldsymbol{x}, \boldsymbol{u}, t)$.

In the fluid limit ($\lambda \ll L$), the collision term causes $f(\boldsymbol{u})$ to approach a Maxwellian velocity distribution while locally conserving mass, momentum, and energy. This property allows us to coarse grain the information in phase space and distill the essential pieces of information, namely how density, mean velocity, and velocity dispersion change as a function of $\boldsymbol{x}$ and t. In practice, this is done by taking the appropriate moments of the Boltzmann equation and integrating over velocity space, d^3u. We identify the mass density

$$\rho = \rho(\boldsymbol{x}, t) = \int m f(\boldsymbol{x}, \boldsymbol{u}, t)\, \mathrm{d}^3u. \tag{10.9}$$

The mass-weighted average of some quantity q at position $\boldsymbol{x}$ is given by

$$\langle q \rangle = \frac{1}{\rho} \int q m f(\boldsymbol{x}, \boldsymbol{u}, t)\, \mathrm{d}^3u. \tag{10.10}$$

10.1.3 Mass conservation – continuity equation

We multiply (10.8) by m and integrate over d^3u to get

$$\begin{aligned} \frac{\partial}{\partial t} \int m f \mathrm{d}^3u + \sum_{i=1}^{3} \frac{\partial}{\partial x_i} \int m f u_i \mathrm{d}^3u \\ + m \int \sum_{i=1}^{3} \frac{\partial}{\partial u_i} (g_i f) \mathrm{d}^3u = \int m \left.\frac{\partial f}{\partial t}\right|_{\mathrm{c}} \mathrm{d}^3u. \end{aligned} \tag{10.11}$$

Here we assume that the force $\boldsymbol{g}$ does not depend on velocity $\boldsymbol{u}$.

Using the definitions (10.9) and (10.10) and applying Gauss' divergence theorem, this simplifies to

$$\frac{\partial}{\partial t} \rho(\boldsymbol{x}, t) + \sum_{i=1}^{3} \frac{\partial}{\partial x_i} \left(\rho \langle u_i \rangle\right) + m \int_{\partial\Omega} f(\boldsymbol{g} \cdot \boldsymbol{n}) \mathrm{d}^2 A_u = 0, \tag{10.12}$$

where $\boldsymbol{n}$ is the normal vector of the differential surface element d^2A_u. The right-hand side vanishes because of local mass conservation: collisions do not create or destroy

particles at a fixed position, they can only discontinuously shift them in velocity space. Since the velocity can be split into a mean and a random component, $\boldsymbol{u} = \boldsymbol{v} + \boldsymbol{w}$, we have $\langle \boldsymbol{u} \rangle \equiv \boldsymbol{v}$ in the second term. Assuming that $f \to 0$ for $|\boldsymbol{u}| \to \infty$, the third term also vanishes on taking the limit of the integration boundary to infinity. We hence obtain

$$\frac{\partial \rho}{\partial t} + \boldsymbol{\nabla} \cdot (\rho \boldsymbol{v}) = 0. \tag{10.13}$$

Taking the volume integral extending over the entire space and applying Gauss' divergence theorem, we can demonstrate that the total mass of the system is conserved:

$$\begin{aligned} \frac{\partial}{\partial t} \int_\Omega \rho \mathrm{d}^3 x + \int_\Omega \boldsymbol{\nabla} \cdot (\rho \boldsymbol{v}) \mathrm{d}^3 x &= 0, \\ \frac{\partial m}{\partial t} + \lim_{\partial\Omega \to \infty} \int_{\partial\Omega} \rho (\boldsymbol{v} \cdot \boldsymbol{n}) \mathrm{d}^2 A &= \frac{\mathrm{d}m}{\mathrm{d}t} = 0. \end{aligned} \tag{10.14}$$

In the last line, we exchanged the total for the partial time derivatives since m depends neither on position nor on velocity.

10.1.4 Momentum conservation

We multiply (10.8) by $m\boldsymbol{u}$ and integrate over $\mathrm{d}^3 u$ to get

$$\begin{aligned} \frac{\partial}{\partial t} \int m u_j f \mathrm{d}^3 u + \sum_{i=1}^{3} \frac{\partial}{\partial x_i} \int m f u_j u_i \mathrm{d}^3 u \\ + m \int \sum_{i=1}^{3} g_i u_j \frac{\partial f}{\partial u_i} \mathrm{d}^3 u = \int m u_j \left. \frac{\partial f}{\partial t} \right|_{\mathrm{c}} d^3 u. \end{aligned} \tag{10.15}$$

The first term is $\partial(\rho v_j)/\partial t$ and second term is

$$\sum_{i=1}^{3} \frac{\partial}{\partial x_i} (\rho \langle u_j u_i \rangle) = \sum_{i=1}^{3} \frac{\partial}{\partial x_i} (\rho v_j v_i + \rho \langle w_j w_i \rangle). \tag{10.16}$$

To simplify the third term, we use the identity

$$\frac{\partial}{\partial u_i} (u_j f) \equiv u_j \frac{\partial f}{\partial u_i} + \delta_{ij} f \tag{10.17}$$

and obtain

$$\sum_{i=1}^{3} m g_i \int \left[\frac{\partial}{\partial u_i} (u_j f) - \delta_{ij} f \right] d^3 u = - \sum_{i=1}^{3} g_i \delta_{ij} \int m f \mathrm{d}^3 u = -\rho g_j, \tag{10.18}$$

where $\delta_{ij} \equiv 1$ for $i = j$, 0 for $i \neq j$ and the first term in the bracket vanishes because of Gauss' divergence theorem. The right-hand side of (10.15) vanishes because collisions conserve momentum.

We get the result

$$\frac{\partial}{\partial t}(\rho v_j) + \sum_{i=1}^{3} \frac{\partial}{\partial x_i}(\rho v_j v_i + \rho\langle w_j w_i\rangle) = \rho g_j. \tag{10.19}$$

The diagonal terms of $\langle w_i w_j\rangle$ are generally much larger than the off-diagonal terms since random velocities in different directions are almost uncorrelated. It is useful to split the $\rho\langle w_i w_j\rangle$ term into an (isotropic) contribution from pressure, P, and a contribution from the anisotropic viscous stress tensor, $\mathbf{\Pi}$,

$$P \equiv \frac{1}{3}\rho\langle|\boldsymbol{w}|^2\rangle, \tag{10.20}$$

$$\Pi_{ij} \equiv P\delta_{ij} - \rho\langle w_i w_j\rangle, \tag{10.21}$$

which is a symmetric and traceless tensor.

The final result is the Navier-Stokes equation

$$\frac{\partial}{\partial t}(\rho v_j) + \sum_{i=1}^{3} \frac{\partial}{\partial x_i}\left(\rho v_i v_j + P\delta_{ij} - \Pi_{ij}\right) = \rho g_j, \text{ or} \tag{10.22}$$

$$\frac{\partial}{\partial t}(\rho\boldsymbol{v}) + \boldsymbol{\nabla}\cdot\left(\rho\boldsymbol{v}\boldsymbol{v}^{\mathrm{T}} + P\mathbf{1} - \mathbf{\Pi}\right) = \rho\boldsymbol{g}, \tag{10.23}$$

where $\mathbf{1}$ is the unit matrix. Taking the volume integral and applying Gauss' divergence theorem (as in 10.14), we can demonstrate that the total momentum, $\boldsymbol{p} = \int \rho\boldsymbol{v}\mathrm{d}^3x$ is conserved in the absence of an external force field that acts as a source of momentum.

To simplify this equation, we rewrite the first two terms in (10.23),

$$\begin{aligned}
&\frac{\partial}{\partial t}(\rho\boldsymbol{v}) + \boldsymbol{\nabla}\cdot\left(\rho\boldsymbol{v}\boldsymbol{v}^{\mathrm{T}}\right) \\
&= \dot{\rho}\boldsymbol{v} + \rho\dot{\boldsymbol{v}} + \rho\boldsymbol{v}(\boldsymbol{\nabla}\cdot\boldsymbol{v}) + \rho(\boldsymbol{v}\cdot\nabla)\boldsymbol{v} + \boldsymbol{v}(\boldsymbol{v}\cdot\boldsymbol{\nabla}\rho) \\
&= \boldsymbol{v}\left[\dot{\rho} + \boldsymbol{\nabla}\cdot(\rho\boldsymbol{v})\right] + \rho\left[\dot{\boldsymbol{v}} + (\boldsymbol{v}\cdot\boldsymbol{\nabla})\boldsymbol{v}\right] = \rho\left[\dot{\boldsymbol{v}} + (\boldsymbol{v}\cdot\boldsymbol{\nabla})\boldsymbol{v}\right].
\end{aligned} \tag{10.24}$$

In the last step, we have used the continuity equation (10.13).

If we use this result in combination with the momentum equation (10.23), we get

$$\frac{\partial\boldsymbol{v}}{\partial t} + (\boldsymbol{v}\cdot\boldsymbol{\nabla})\boldsymbol{v} = \boldsymbol{g} - \frac{1}{\rho}\boldsymbol{\nabla}P + \frac{1}{\rho}\boldsymbol{\nabla}\cdot\mathbf{\Pi}. \tag{10.25}$$

Viscosity acts to oppose shearing motion and interpenetration.

To make progress, we adopt an ansatz for the viscous stress tensor and assume a "Newtonian fluid", i.e., we assume that Π_{ij} is linearly proportional to the velocity gradient, $\partial v_i/\partial x_j$. The most general symmetric tensor that is linear in $\partial v_i/\partial x_j$ is

$$\Pi_{ij} = \eta D_{ij} + \xi \delta_{ij} (\boldsymbol{\nabla} \cdot \boldsymbol{v}), \text{ where} \tag{10.26}$$

$$D_{ij} = \frac{\partial v_i}{\partial x_j} + \frac{\partial v_j}{\partial x_i} - \frac{2}{3} \delta_{ij} (\boldsymbol{\nabla} \cdot \boldsymbol{v}) \tag{10.27}$$

is the deformation tensor that vanishes for uniform expansion or contraction. η and ξ are the coefficients of shear and bulk viscosity, respectively and have units of $\mathrm{g\ cm^{-1}\ s^{-1}}$. The term ηD_{ij} represents resistance to shearing motion and $\xi \delta_{ij} (\boldsymbol{\nabla} \cdot \boldsymbol{v})$ represents resistance to changes in volume.

10.1.5 Energy conservation

To obtain the internal energy equation, we multiply (10.8) by $m\boldsymbol{u}^2$ and integrate over $\mathrm{d}^3 u$. Making use of Gauss' divergence theorem and of the fact that collisions conserve energy (as well as mass and momentum) we get (after a similar procedure)

$$\begin{aligned} \rho \frac{\mathrm{d}e_{\mathrm{th}}}{\mathrm{d}t} &\equiv \rho \left(\frac{\partial e_{\mathrm{th}}}{\partial t} + \boldsymbol{v} \cdot \boldsymbol{\nabla} e_{\mathrm{th}} \right) \\ &= \frac{\partial}{\partial t} (\rho e_{\mathrm{th}}) + \boldsymbol{\nabla} \cdot (\rho e_{\mathrm{th}} \boldsymbol{v}) = -P \boldsymbol{\nabla} \cdot \boldsymbol{v} + \Psi - \boldsymbol{\nabla} \cdot \boldsymbol{Q}. \end{aligned} \tag{10.28}$$

In the second step, we have used the continuity equation (10.13). Here, e_{th} is the specific internal energy (10.1), Ψ is the viscous dissipation rate, and $\boldsymbol{Q}$ is the conductive heat flux:

$$e_{\mathrm{th}} \equiv \frac{1}{2} \left\langle |\boldsymbol{w}|^2 \right\rangle, \tag{10.29}$$

$$\Psi \equiv \sum_{i,j=1}^{3} \Pi_{ij} \frac{\partial v_i}{\partial x_j} = \boldsymbol{\Pi} : \boldsymbol{\nabla} \boldsymbol{v}, \tag{10.30}$$

$$\boldsymbol{Q} \equiv \frac{1}{2} \rho \left\langle \boldsymbol{w} |\boldsymbol{w}|^2 \right\rangle. \tag{10.31}$$

Ψ represents conversion of bulk motion of the fluid into internal energy via viscous dissipation. It is the viscous analog of heating by $P\mathrm{d}V$ work.

If the distribution of the random velocity component, $\boldsymbol{w}$, is symmetric about zero, then $\boldsymbol{Q}$ vanishes. If the distribution is skewed, then hot particles drift relative to cold particles and produce a heat flux in the direction of the drift. In most cases, a temperature gradient produces a conductive flux,

$$\boldsymbol{Q} = -\chi \boldsymbol{\nabla} T, \quad \text{with } \chi \simeq 6 \times 10^{-7}\, T^{5/2}\, \mathrm{erg\ s^{-1} cm^{-1} K^{-1}}. \tag{10.32}$$

We will also use $\kappa = \chi T/P$ instead of χ for convenience (κ has units of cm^2 s^{-1}, i.e., of a diffusion coefficient). However, if $\boldsymbol{Q}$ is uniform, heat flowing out is replaced by heat flowing in. Hence, the local thermal energy changes only if $\boldsymbol{\nabla} \cdot \boldsymbol{Q} \neq 0$.

Since we are interested how the total energy density, $\rho \boldsymbol{v}^2/2 + \rho e_{\rm th}$, changes in a given volume, we are supplementing the internal energy equation (10.28) with a conservation law of $\rho \boldsymbol{v}^2/2$. To this end, we consider

$$\frac{\partial}{\partial t}\left(\frac{\rho \boldsymbol{v}^2}{2}\right) = \frac{\boldsymbol{v}^2}{2}\frac{\partial \rho}{\partial t} + \rho \boldsymbol{v} \cdot \frac{\partial \boldsymbol{v}}{\partial t} \tag{10.33}$$

and substitute equations (10.13) and (10.25) to get

$$\frac{\partial}{\partial t}\left(\frac{\rho \boldsymbol{v}^2}{2}\right) = -\frac{\boldsymbol{v}^2}{2}\boldsymbol{\nabla} \cdot (\rho \boldsymbol{v}) - \rho \boldsymbol{v} \cdot (\boldsymbol{v} \cdot \boldsymbol{\nabla})\boldsymbol{v} + \rho \boldsymbol{v} \cdot \boldsymbol{g} - \boldsymbol{v} \cdot \boldsymbol{\nabla} P + \boldsymbol{v} \cdot (\boldsymbol{\nabla} \cdot \boldsymbol{\Pi}). \tag{10.34}$$

Using the identity $(\boldsymbol{v} \cdot \boldsymbol{\nabla})\boldsymbol{v} \equiv \boldsymbol{\nabla}\boldsymbol{v}^2/2$, we obtain an equation for the conservation of kinetic energy density

$$\frac{\partial}{\partial t}\left(\frac{\rho \boldsymbol{v}^2}{2}\right) + \boldsymbol{\nabla} \cdot \left(\frac{1}{2}\rho \boldsymbol{v}^2 \boldsymbol{v}\right) = \rho \boldsymbol{v} \cdot \boldsymbol{g} - \boldsymbol{v} \cdot \boldsymbol{\nabla} P + \boldsymbol{v} \cdot (\boldsymbol{\nabla} \cdot \boldsymbol{\Pi}). \tag{10.35}$$

Combining equations (10.35) and (10.28), we arrive at the evolution equation for the total specific energy, $e = e_{\rm th} + \boldsymbol{v}^2/2$,

$$\frac{\partial}{\partial t}(\rho e) + \boldsymbol{\nabla} \cdot [(\rho e + P)\boldsymbol{v} - \boldsymbol{\Pi} \cdot \boldsymbol{v} + \boldsymbol{Q}] = \rho \boldsymbol{v} \cdot \boldsymbol{g}. \tag{10.36}$$

Taking the volume integral over the entire space and applying Gauss' divergence theorem, we can demonstrate that the total energy in a system is conserved if there are no external forces $\boldsymbol{g}$ acting on our fluid.

10.1.6 Entropy conservation

One can derive an equivalent equation for the entropy by considering the first law of thermodynamics,

$$\mathrm{d}e_{\rm th} = -P\mathrm{d}\tilde{V} + T\mathrm{d}s = \frac{P}{\rho^2}\mathrm{d}\rho + T\mathrm{d}s, \tag{10.37}$$

where $\tilde{V} = \rho^{-1}$ is the specific volume. Combining this with the internal energy equation (10.28), we get

$$\frac{P}{\rho^2}\frac{\mathrm{d}\rho}{\mathrm{d}t} + T\frac{\mathrm{d}s}{\mathrm{d}t} = -\frac{P}{\rho}\boldsymbol{\nabla} \cdot \boldsymbol{v} - \frac{1}{\rho}\boldsymbol{\nabla} \cdot \boldsymbol{Q} + \frac{1}{\rho}\Psi. \tag{10.38}$$

Using the continuity equation, $\mathrm{d}\rho/\mathrm{d}t = -\rho\boldsymbol{\nabla}\cdot\boldsymbol{v}$, the first terms on both sides cancel each other and we obtain,

$$\rho T\frac{\mathrm{d}s}{\mathrm{d}t} \;=\; -\boldsymbol{\nabla}\cdot\boldsymbol{Q}+\Psi. \tag{10.39}$$

This shows explicitly, that heat conduction and viscous friction change the entropy. Equivalently, if these processes are absent, specific entropy is conserved.

10.2 Euler and Navier-Stokes equations

The gas flows in astrophysics are often of extremely low density, making internal friction in the gas extremely small. In the limit of assuming internal friction and heat conduction to be completely absent, we arrive at the so-called ideal gas dynamics as described by the Euler equations. Most calculations in cosmology and galaxy formation are carried out under this assumption. However, in certain regimes, viscosity may still become important (for example in the very hot plasma of rich galaxy clusters), hence we shall also briefly discuss the hydrodynamical equations in the presence of physical viscosity, the Navier-Stokes equations, which in a sense describe *real* fluids as opposed to ideal ones. Phenomena such as fluid instabilities or turbulence are also best understood if one does not neglect viscosity completely.

10.2.1 Euler equations

If internal friction and heat conduction in a gas flow can be neglected, the dynamics of the fluid is governed by the Euler equations (Eqns. (10.13), (10.23), and (10.36) for vanishing viscosity, conductivity, and external forces):

$$\frac{\partial\rho}{\partial t}+\boldsymbol{\nabla}\cdot(\rho\boldsymbol{v})=0, \tag{10.40}$$

$$\frac{\partial}{\partial t}(\rho\boldsymbol{v})+\boldsymbol{\nabla}\cdot(\rho\boldsymbol{v}\boldsymbol{v}^T+P\mathbf{1})=0, \tag{10.41}$$

$$\frac{\partial}{\partial t}(\rho e)+\boldsymbol{\nabla}\cdot[(\rho e+P)\boldsymbol{v}]=0, \tag{10.42}$$

where $e = e_{\mathrm{th}} + \boldsymbol{v}^2/2$ is the total energy per unit mass, and e_{th} is the thermal energy per unit mass. Each of these equations is a continuity law, one for the mass, one for the momentum, and one for the total energy. The equations hence form a set of hyperbolic conservation laws. In the form given above, they are not yet complete, however. One still needs a further expression that gives the pressure in terms of the other thermodynamic variables. For an ideal gas, the pressure law is

$$P=(\gamma-1)\rho e_{\mathrm{th}}, \tag{10.43}$$

where $\gamma = c_p/c_v$ is the ratio of specific heats. For a monoatomic gas, we have $\gamma = 5/3$.

10.2.2 Navier-Stokes equations

Real fluids have internal stresses, due to *viscosity*. The effect of viscosity is to dissipate relative motions of the fluid into heat. The Navier-Stokes equations are then given by (Eqns. (10.13), (10.23), and (10.36) for vanishing conductivity and external forces)

$$\frac{\partial \rho}{\partial t} + \boldsymbol{\nabla} \cdot (\rho \boldsymbol{v}) = 0, \tag{10.44}$$

$$\frac{\partial}{\partial t}(\rho \boldsymbol{v}) + \boldsymbol{\nabla} \cdot (\rho \boldsymbol{v}\boldsymbol{v}^T + P\mathbf{1}) = \boldsymbol{\nabla} \cdot \boldsymbol{\Pi}, \tag{10.45}$$

$$\frac{\partial}{\partial t}(\rho e) + \boldsymbol{\nabla} \cdot [(\rho e + P)\boldsymbol{v}] = \boldsymbol{\nabla} \cdot (\boldsymbol{\Pi} \cdot \boldsymbol{v}). \tag{10.46}$$

Here, $\boldsymbol{\Pi}$ is the so-called viscous stress tensor, which is a material property. For $\boldsymbol{\Pi} = \mathbf{0}$, the Euler equations are recovered. To first order, the viscous stress tensor must be a linear function of the velocity derivatives (Landau & Lifshitz, 1959). The most general tensor of rank-2 of this type can be written as

$$\boldsymbol{\Pi} = \eta \left[\boldsymbol{\nabla}\boldsymbol{v} + (\boldsymbol{\nabla}\boldsymbol{v})^T - \frac{2}{3}(\boldsymbol{\nabla} \cdot \boldsymbol{v})\mathbf{1} \right] + \xi(\boldsymbol{\nabla} \cdot \boldsymbol{v})\mathbf{1}. \tag{10.47}$$

Here η scales the traceless part of the tensor and describes the shear viscosity. ξ gives the strength of the diagonal part, and is the so-called bulk viscosity. Note that η and ξ can in principle be functions of local fluid properties, such as ρ, T, etc.

Incompressible fluids

In the following we shall assume constant viscosity coefficients. Also, we specialize to incompressible fluids with $\boldsymbol{\nabla} \cdot \boldsymbol{v} = 0$, which is a particularly important case in practice. Let's see how the Navier-Stokes equations simplify in this case. Obviously, ξ is then unimportant and we only need to deal with shear viscosity. Now, let us consider one of the components of the viscous shear force described by equation (10.45):

$$\begin{aligned} \frac{1}{\eta}(\boldsymbol{\nabla} \cdot \boldsymbol{\Pi})_x &= \frac{\partial}{\partial x}\left(2\frac{\partial v_x}{\partial x}\right) + \frac{\partial}{\partial y}\left(\frac{\partial v_x}{\partial y} + \frac{\partial v_y}{\partial x}\right) + \frac{\partial}{\partial z}\left(\frac{\partial v_x}{\partial z} + \frac{\partial v_z}{\partial x}\right) \\ &= \left(\frac{\partial^2}{\partial x^2} + \frac{\partial^2}{\partial y^2} + \frac{\partial^2}{\partial z^2}\right) v_x = \boldsymbol{\nabla}^2 v_x, \end{aligned} \tag{10.48}$$

where we made use of the $\boldsymbol{\nabla} \cdot \boldsymbol{v} = 0$ constraint. If we furthermore introduce the *kinematic viscosity* ν as

$$\nu \equiv \frac{\eta}{\rho}, \tag{10.49}$$

we can write the equivalent of equation (10.45) in the compact form

$$\frac{\mathrm{d}\,\boldsymbol{v}}{\mathrm{d}\,t} = -\frac{\boldsymbol{\nabla} P}{\rho} + \nu \boldsymbol{\nabla}^2 \boldsymbol{v}, \tag{10.50}$$

where the derivative on the left-hand side is the Lagrangian derivative,

$$\frac{\mathrm{d}}{\mathrm{d}\,t} = \frac{\partial}{\partial t} + \boldsymbol{v} \cdot \boldsymbol{\nabla}. \tag{10.51}$$

We hence see that the motion of individual fluid elements responds to pressure gradients and to viscous forces. The form (10.50) of the equation is also often simply referred to as the Navier-Stokes equation.

10.2.3 Scaling properties of viscous flows

Consider the Navier-Stokes equations for some flow problem that is characterized by some characteristic length L_0, velocity V_0, and density scale ρ_0. We can then define dimensionless fluid variables of the form

$$\hat{\boldsymbol{v}} = \frac{\boldsymbol{v}}{V_0}, \qquad \hat{\boldsymbol{x}} = \frac{\boldsymbol{x}}{L_0}, \qquad \hat{P} = \frac{P}{\rho_0 V_0^2}. \tag{10.52}$$

Similarly, we define a dimensionless time, a dimensionless density, and a dimensionless Nabla operator:

$$\hat{t} = \frac{t}{L_0/V_0}, \qquad \hat{\rho} = \frac{\rho}{\rho_0}, \qquad \hat{\boldsymbol{\nabla}} = L_0 \boldsymbol{\nabla}. \tag{10.53}$$

Inserting these definitions into the Navier-Stokes equation (10.50), we obtain the dimensionless equation

$$\frac{\mathrm{d}\hat{\boldsymbol{v}}}{\mathrm{d}\hat{t}} = -\frac{\hat{\boldsymbol{\nabla}} \hat{P}}{\hat{\rho}} + \frac{\nu}{L_0 V_0} \hat{\boldsymbol{\nabla}}^2 \hat{\boldsymbol{v}}. \tag{10.54}$$

Interestingly, this equation involves one number,

$$\mathrm{Re} \equiv \frac{L_0 V_0}{\nu}, \tag{10.55}$$

which characterizes the flow and determines the structure of the possible solutions of the equation. This is the so-called Reynolds number. Problems which have similar Reynolds number are expected to exhibit very similar fluid behavior. One then has *Reynolds-number similarity*. In contrast, the Euler equations ($\mathrm{Re} \to \infty$) exhibit always scale similarity because they are invariant under scale transformations.

One intuitive interpretation one can give the Reynolds number is that it measures the importance of inertia relative to viscous forces. Hence:

$$\mathrm{Re} \approx \frac{\text{inertial forces}}{\text{viscous forces}} \approx \frac{D\boldsymbol{v}/Dt}{\nu\boldsymbol{\nabla}^2\boldsymbol{v}} \approx \frac{V_0/(L_0/V_0)}{\nu V_0/L_0^2} = \frac{L_0 V_0}{\nu}. \tag{10.56}$$

If we have $\mathrm{Re} \sim 1$, we are completely dominated by viscosity. On the other hand, for $\mathrm{Re} \to \infty$ viscosity becomes unimportant and we approach an ideal gas.

10.3 Shocks

An important feature of hydrodynamical flows is that they can develop shock waves in which the density, velocity, temperature and specific entropy jump by finite amounts (e.g. Toro, 1997). In the case of the Euler equations, such shocks are true mathematical discontinuities while they exhibit a finite width for the Navier-Stokes equations.

10.3.1 General considerations

Imagine the propagation of a sound wave with finite amplitude. The sound speed is higher at higher temperature as $c_\mathrm{s}^2 = \gamma k_\mathrm{B} T/(\mu m_\mathrm{p})$ where μ is the mean molecular weight so that the crest of the wave gradually overtakes the colder trough ($T \propto \rho^{\gamma-1}$). When faster moving gas overtakes slower moving gas, we would obtain a multivalued solution that is inconsistent with the hydrodynamic equations. Instead, we get a discontinuous change of density and velocity, a so-called "shock". This steepening happens even for isothermal gas ($\gamma = 1$) because of the non-linearity of the equations. Shocks can also be produced by any supersonic compressible disturbance (or through non-linear interactions of subsonic compressible modes). This can result from a supernova explosion within a galaxy, by gas accreting super-sonically onto a galaxy cluster, or if two galaxies or even galaxy clusters merge to form a larger entity. In general, a shock wave is

1. propagating faster than the "signal speed" for compressible waves, c_s,
2. producing an irreversible change of the fluid state, i.e., an increase in entropy, and
3. can either be caused by a pressure-driven compressive disturbance, results from non-linear wave interactions, or is caused by supersonic collisions of two streams of fluids (e.g., as a result of their mutual gravitational interactions).

In most cases, a shock involves a "discontinuous" change of the fluid properties over a scale proportional to the effective mean free path λ_eff. In "collisional" shocks, λ is set

by Coulomb-force mediated particle-particle collisions (in air the mean free path is of order μm). In a "collisionless" plasma (the solar wind, the interstellar and intracluster media) electromagnetic viscosities mediate interactions between charged particles and thus reduce $\lambda_{\rm eff}$ by many orders of magnitude, $\lambda_{\rm eff} \ll \lambda_{\rm Coulomb}$, so that we are dealing here with "collisionless" shocks.

In order to understand general properties at fluid discontinuities, we are now considering the conservation laws of mass, momentum, thermal and kinetic energy (Eqns. (10.13), (10.25), (10.28), and (10.34)) in the absence of external gravitational forces and conductive heat flux, which act on time scale that are much longer in comparison to the transition time at shocks,

$$\frac{\partial \rho}{\partial t} + \boldsymbol{\nabla} \cdot (\rho \boldsymbol{v}) = 0, \tag{10.57}$$

$$\frac{\partial \boldsymbol{v}}{\partial t} + (\boldsymbol{v} \cdot \boldsymbol{\nabla})\boldsymbol{v} = -\frac{\boldsymbol{\nabla} P}{\rho} + \frac{1}{\rho}\boldsymbol{\nabla} \cdot \boldsymbol{\Pi} \tag{10.58}$$

$$\frac{\partial}{\partial t}(\rho e_{\rm th}) + \boldsymbol{\nabla} \cdot (\rho e_{\rm th} \boldsymbol{v}) = -P \boldsymbol{\nabla} \cdot \boldsymbol{v} + \Psi, \tag{10.59}$$

$$\frac{\partial}{\partial t}\left(\frac{\rho \boldsymbol{v}^2}{2}\right) + \boldsymbol{\nabla} \cdot \left(\frac{1}{2}\rho \boldsymbol{v}^2 \boldsymbol{v}\right) = -\boldsymbol{v} \cdot \boldsymbol{\nabla} P + \boldsymbol{v} \cdot (\boldsymbol{\nabla} \cdot \boldsymbol{\Pi}). \tag{10.60}$$

10.3.2 Jump conditions

Consider a propagating fluid discontinuity in the rest frame of the discontinuity. Fluid moves from upstream to downstream. We denote the *upstream conditions* by ρ_1, v_1, T_1 and *downstream conditions* by ρ_2, v_2, T_2.

We would like to derive the relations (also known as "jump conditions") between ρ_1, v_1, T_1 and ρ_2, v_2, T_2 for a steady-state, plane-parallel geometry of a fluid discontinuity such as a shock. First, we assume that the velocity is perpendicular to the surface of the discontinuity. While this may seem to be a substantial loss of generality, it captures the main effect of discontinuities as we will see by generalizing this simplification in the last part of this section. As we will also see, there are two types of discontinuities:

1. shocks that are characterized by a mass flux through their interface, and
2. contact discontinuities which have *no* mass flux through their interface.

Within the shock front or "transition layer" on a scale of $\lambda_{\rm eff}$, viscous effects are important and cause the shock in the first place, i.e., dissipate kinetic energy and thus generate heat and entropy. However, outside the layer, viscous effects are small on scales $L \gg \lambda_{\rm eff}$. We will derive conservation equations of the form

$$\frac{\rm d}{{\rm d}x} Q(\rho, v, P) = 0 \implies Q(\rho, v, P) = \text{const.} \tag{10.61}$$

and although Q involves viscous terms, we can ignore these outside the shock zone and can derive jump conditions from equations without viscosity terms.

We assume steady state ($\partial/\partial t = 0$) and plane-parallel geometry ($\partial/\partial y = \partial/\partial z = 0$, $\partial/\partial x = \mathrm{d}/\mathrm{d}x$). The conservation laws (10.57), (10.58), (10.59), and (10.60) simplify to yield

$$\frac{\mathrm{d}}{\mathrm{d}x}(\rho v) = 0, \tag{10.62}$$

$$v\frac{\mathrm{d}v}{\mathrm{d}x} = -\frac{1}{\rho}\frac{\mathrm{d}P}{\mathrm{d}x} + \frac{1}{\rho}\frac{\mathrm{d}}{\mathrm{d}x}\left\{\left(\frac{4}{3}\eta + \xi\right)\frac{\mathrm{d}v}{\mathrm{d}x}\right\}, \tag{10.63}$$

$$\frac{\mathrm{d}}{\mathrm{d}x}(\rho e_{\mathrm{th}} v) = -P\frac{\mathrm{d}u}{\mathrm{d}x} + \left(\frac{4}{3}\eta + \xi\right)\left(\frac{\mathrm{d}v}{\mathrm{d}x}\right)^2, \tag{10.64}$$

$$\frac{\mathrm{d}}{\mathrm{d}x}\left(\frac{1}{2}\rho v^2 v\right) = -v\frac{\mathrm{d}P}{\mathrm{d}x} + v\frac{\mathrm{d}}{\mathrm{d}x}\left\{\left(\frac{4}{3}\eta + \xi\right)\frac{\mathrm{d}v}{\mathrm{d}x}\right\}. \tag{10.65}$$

The equation for mass conservation (10.62) gives

$$\rho v = \text{const.} \implies \rho_1 v_1 = \rho_2 v_2 = j \implies [\rho v] = 0, \tag{10.66}$$

where j is the current density and we introduced the abbreviation $[q] = q_2 - q_1$ for the difference between the up- and downstream quantities q_i. Note, that the up- and downstream velocities, v_1 and v_2, are measured in the frame of the discontinuity!

Using

$$\frac{\mathrm{d}}{\mathrm{d}x}\left(\rho v^2\right) = \rho v\frac{\mathrm{d}v}{\mathrm{d}x} + v\frac{\mathrm{d}}{\mathrm{d}x}(\rho v) \overset{(10.61)}{=} \rho v\frac{\mathrm{d}v}{\mathrm{d}x} \tag{10.67}$$

allows (10.63) to be rewritten as

$$\rho v\frac{\mathrm{d}v}{\mathrm{d}x} + \frac{\mathrm{d}P}{\mathrm{d}x} - \frac{\mathrm{d}}{\mathrm{d}x}\left\{\left(\frac{4}{3}\eta + \xi\right)\frac{\mathrm{d}v}{\mathrm{d}x}\right\}$$

$$= \frac{\mathrm{d}}{\mathrm{d}x}\left\{\rho v^2 + P - \left(\frac{4}{3}\eta + \xi\right)\frac{\mathrm{d}v}{\mathrm{d}x}\right\} = 0 \tag{10.68}$$

$$\implies \left[\rho v^2 + P - \left(\frac{4}{3}\eta + \xi\right)\frac{\mathrm{d}v}{\mathrm{d}x}\right] = 0 \tag{10.69}$$

This demonstrates that within the transition zone (where η, ξ, and $\mathrm{d}v/\mathrm{d}x$ are non-zero) $\rho v^2 + P \neq$ const. However, in the pre- and post-shock zones, η, ξ, and $\mathrm{d}v/\mathrm{d}x$ are negligible, implying

$$\left[\rho v^2 + P\right] = 0. \tag{10.70}$$

In principle, we could use (10.69) to follow the behavior in the transition zone, i.e., to understand how entropy is generated. But on scales $L < \lambda$ the fluid description breaks

down and we have to reside to kinetic theory (or use plasma particle-in-cell codes to understand the nonlinear behavior of the heating process). From now on, we neglect viscosity effects in the bulk.

Adding (10.64) and (10.65) yields (for the region outside the transition zone)

$$\begin{aligned} 0 &= \frac{\mathrm{d}}{\mathrm{d}x}\left\{v\left(\frac{1}{2}\rho v^2 + \rho e_{\mathrm{th}}\right) + Pv\right\} = \frac{\mathrm{d}}{\mathrm{d}x}\left\{\rho v\left(\frac{1}{2}v^2 + e_{\mathrm{th}} + \frac{P}{\rho}\right)\right\} \\ &= \left(\frac{1}{2}v^2 + e_{\mathrm{th}} + \frac{P}{\rho}\right)\frac{\mathrm{d}}{\mathrm{d}x}(\rho v) + \rho v \frac{\mathrm{d}}{\mathrm{d}x}\left(\frac{1}{2}v^2 + e_{\mathrm{th}} + \frac{P}{\rho}\right). \end{aligned} \tag{10.71}$$

Since $\mathrm{d}(\rho v)/\mathrm{d}x = 0$ and $\rho v \neq 0$, we obtain

$$\frac{\mathrm{d}}{\mathrm{d}x}\left(\frac{1}{2}v^2 + e_{\mathrm{th}} + \frac{P}{\rho}\right) = 0 \implies \left[\frac{1}{2}v^2 + e_{\mathrm{th}} + \frac{P}{\rho}\right] = 0. \tag{10.72}$$

Summarizing, we have the Rankine-Hugoniot jump conditions for a plane-parallel shock in the shock rest frame:

$$[\rho v] = 0, \tag{10.73}$$

$$\left[\rho v^2 + P\right] = 0, \tag{10.74}$$

$$\left[\frac{1}{2}v^2 + e_{\mathrm{th}} + \frac{P}{\rho}\right] = 0. \tag{10.75}$$

Independent of the complicated physics within the transition layer, these conditions simply follow from the conservation laws. The first follows from mass conservation, the second from mass and momentum conservation, and the third from mass and total energy conservation.

Using $e_{\mathrm{th},i} = P_i/\{\rho_i(\gamma_i - 1)\}$, we can rewrite the energy jump condition to get

$$\frac{1}{2}v_1^2 + \frac{\gamma_1}{\gamma_1 - 1}\frac{P_1}{\rho_1} = \frac{1}{2}v_2^2 + \frac{\gamma_2}{\gamma_2 - 1}\frac{P_2}{\rho_2} \tag{10.76}$$

for a single-species gas that is described by a polytropic equation of state. In principle, $\gamma_1 \neq \gamma_2$, since a shock can e.g., dissociate molecules, or raise T so that previously inaccessible degrees of freedom become accessible.

10.3.3 Tangential discontinuities

$[\rho v] = 0$ allows for two types of solutions. The first type is clearly $\rho_1 v_1 = \rho_2 v_2 = 0$ and since ρ_1 and ρ_2 are non-zero, we have

$$v_1 = v_2 = 0, \tag{10.77}$$

$$P_1 = P_2 \implies [P] = 0 \tag{10.78}$$

which follows from (10.74). The constancy of the normal component of the velocity across such an interface implies that there is no mass flux through a tangential discontinuity. If additionally the tangential velocity is also continuous, a special discontinuity is present which is called a contact discontinuity.

At a tangential discontinuity, there can be an arbitrary jump of density, that however needs to be compensated by the same jump of T, but in the opposite direction!

10.3.4 Shock Mach number

The other type of solution requires $\rho_1 v_1 \neq 0$ so that we have a mass flux through this type of discontinuity that we call a "shock".

We define a dimensionless number that characterizes the shock strength, the Mac number as the ratio of shock speed to upstream sound speed $c_1^2 = \gamma P/\rho$,

$$\mathcal{M}_1 \equiv \frac{v_1}{c_1} = \sqrt{\frac{\rho_1 v_1^2}{\gamma P_1}} = \sqrt{\frac{m v_1^2}{\gamma k_{\rm B} T_1}}, \tag{10.79}$$

which can be interpreted as a ratio of ram pressure ($\rho_1 v_1^2$)-to-thermal pressure in the pre-shock gas or equivalently a ratio of kinetic-to-thermal energy density.

We can rewrite the Rankine-Hugoniot jump conditions in terms of $\mathcal{M}_1$ ($\gamma_1 = \gamma_2$)

$$\frac{\rho_2}{\rho_1} = \frac{v_1}{v_2} = \frac{(\gamma+1)\mathcal{M}_1^2}{(\gamma-1)\mathcal{M}_1^2+2} \xrightarrow{\gamma=1} \mathcal{M}_1^2 \tag{10.80}$$

$$\frac{P_2}{P_1} = \frac{\rho_2 k_{\rm B} T_2}{\rho_1 k_{\rm B} T_1} = \frac{2\gamma\mathcal{M}_1^2 - (\gamma-1)}{\gamma+1} \xrightarrow{\gamma=1} \mathcal{M}_1^2 \tag{10.81}$$

$$\frac{T_2}{T_1} = \frac{[(\gamma-1)\mathcal{M}_1^2+2]\,[2\gamma\mathcal{M}_1^2-(\gamma-1)]}{(\gamma+1)^2\mathcal{M}_1^2} \xrightarrow{\gamma=1} 1 \tag{10.82}$$

Those relations simplify for strong shocks ($\mathcal{M} \gg 1$), yielding

$$\frac{\rho_2}{\rho_1} = \frac{v_1}{v_2} \approx \frac{\gamma+1}{\gamma-1} = 4, \tag{10.83}$$

$$P_2 \approx \frac{2\gamma}{\gamma+1}\mathcal{M}_1^2 P_1 = \frac{2}{\gamma+1}\rho_1 v_1^2 = \frac{3}{4}\rho_1 v_1^2, \tag{10.84}$$

$$k_{\rm B} T_2 \approx \frac{2\gamma(\gamma-1)}{(\gamma+1)^2} k_{\rm B} T_1 \mathcal{M}_1^2 = \frac{2(\gamma-1)}{(\gamma+1)^2} m v_1^2 = \frac{3}{16} m v_1^2, \tag{10.85}$$

where we used a non-relativistic ideal gas ($\gamma = 5/3$) in the last equalities.

In the shock rest frame, the post-shock kinetic and thermal specific energies are ($\gamma = 5/3$, $\mathcal{M} \gg 1$)

$$\frac{1}{2}v_2^2 \approx \frac{1}{32}v_1^2, \tag{10.86}$$

$$\frac{3}{2}\frac{k_\mathrm{B}T_2}{m} \approx \frac{9}{32}v_1^2 = \frac{9}{16}\left(\frac{1}{2}v_1^2\right). \tag{10.87}$$

So roughly half of the pre-shock kinetic energy is converted to thermal energy (in the shock rest frame). The total specific energy e_2 of the post-shock gas,

$$e_2 = \frac{1}{2}v_2^2 + \frac{3}{2}\frac{k_\mathrm{B}T_2}{m} \approx \frac{10}{16}\left(\frac{1}{2}v_1^2\right) = \frac{5}{8}e_{\mathrm{kin},1} = \frac{5}{8}e_1 \tag{10.88}$$

is lower (in the shock rest frame) because of the $P\mathrm{d}V$ work done by pressure and viscosity on the post-shock gas in compressing its volume. Note that this $P\mathrm{d}V$ term is absent in the rest frame of the post-shock gas.

The post-shock Mach number is

$$\mathcal{M}_2 \equiv \frac{v_2}{c_2} = \frac{v_1}{c_1}\frac{v_2}{v_1}\frac{c_1}{c_2} = \mathcal{M}_1\frac{v_2}{v_1}\left(\frac{T_1}{T_2}\right)^{1/2}. \tag{10.89}$$

This simplifies in the strong-shock limit, yielding

$$\mathcal{M}_2 \approx \mathcal{M}_1\frac{\gamma-1}{\gamma+1}\left(\frac{(\gamma+1)^2}{2\gamma(\gamma-1)\mathcal{M}_1^2}\right)^{1/2} = \left(\frac{\gamma-1}{2\gamma}\right)^{1/2} \approx 0.45. \tag{10.90}$$

A shock converts supersonic gas into denser, slower moving, higher pressure, subsonic gas.

10.3.5 Shock adiabatic curve

The shock increases the specific entropy of the gas by an amount

$$\begin{aligned} s_2 - s_1 &= c_V \ln\left(\frac{P_2}{\rho_2^\gamma}\right) - c_V \ln\left(\frac{P_1}{\rho_1^\gamma}\right) \\ &= c_V \ln\left(\frac{P_2}{P_1}\right) - c_V\gamma \ln\left(\frac{\rho_2}{\rho_1}\right) = c_V \ln\left(\frac{K_2}{K_1}\right). \end{aligned} \tag{10.91}$$

Hence, the shock shifts the gas to a higher adiabatic curve that is uniquely labeled by $K = P\rho^{-\gamma}$: gas can move adiabatically along an adiabatic curve while changes in entropy move it from one adiabatic curve to another.

With the definition of the current density $j = \rho_1 v_1 = \rho_2 v_2 = \text{const.}$, we obtain for (10.74)

$$[\rho v^2 + P] = \left[\frac{j^2}{m} V + P\right] = 0 \implies \frac{j^2}{m} V_1 + P_1 = \frac{j^2}{m} V_2 + P_2. \tag{10.92}$$

Hence, the slope of the shock adiabatic curve in the P-V diagram is

$$\frac{j^2}{m} = \frac{P_2 - P_1}{V_1 - V_2}. \tag{10.93}$$

10.3.6 Oblique shocks

So far, our specific discussion about shocks has been constrained to plane-parallel shock geometries, i.e., we only considered a fluid velocity that was aligned with the shock normal. In general, the fluid can impact the shock at some oblique angle. We define a velocity component parallel to the shock normal, $v_\parallel \equiv \boldsymbol{v} \cdot \boldsymbol{n}$, as well as a perpendicular component, $v_\perp$.

The momentum conservation equation (10.23) defines a momentum current through a unit surface area with normal vector $\boldsymbol{n}$,

$$\rho \boldsymbol{v} (\boldsymbol{v} \cdot \boldsymbol{n}) + P \boldsymbol{n}. \tag{10.94}$$

The momentum current has to be continuous across the shock in order for the forces that are acting on both sides of the shock on the gas, are identical. In our case, $\boldsymbol{n}$ coincides with the shock normal and points along $\boldsymbol{e}_x$. Continuity of the x, y, and z components of the momentum current yields

$$[\rho v_x^2 + P] = 0, \tag{10.95}$$
$$[\rho v_x v_y] = 0, \tag{10.96}$$
$$[\rho v_x v_z] = 0. \tag{10.97}$$

At a shock $j = \rho v_x \neq 0$ and $\rho \neq 0$ so that we get

$$[v_y] = 0 \quad \text{and} \quad [v_z] = 0, \tag{10.98}$$

i.e., the tangential velocities are continuous across the shock. Thus, only the parallel velocity component is modified at a shock according to $v_{\parallel,2} = v_{\parallel,1} \rho_1 / \rho_2$ while the perpendicular component remains invariant, $v_{\perp,1} = v_{\perp,2} = v_\perp$. This implies a refraction of the (oblique) flow toward the shock surface.

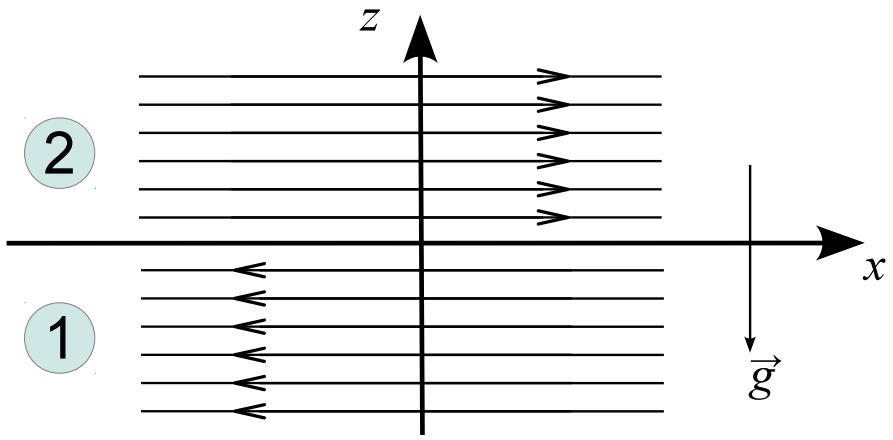

Figure 10.1: Geometry of a generic shear flow.

10.4 Fluid instabilities

In many situations, gaseous flows can be subject to fluid instabilities in which small perturbations can rapidly grow, thereby tapping a source of free energy. An important example of this are Kelvin-Helmholtz and Rayleigh-Taylor instabilities, which we briefly discuss in this section.

10.4.1 Stability of a shear flow

We consider a flow in the x-direction, which in the lower half-space $z < 0$ has velocity v_1 and density ρ_1, whereas in the upper half-space the gas streams with v_2 and has density ρ_2. In addition there can be a homogeneous gravitational field $\boldsymbol{g}$ pointing into the negative z-direction, as sketched in Figure 10.1.

The stability of the flow can be analysed through perturbation theory. To this end, one can for example treat the flow as an incompressible potential flow, and carry out an Eigenmode analysis in Fourier space. With the help of Bernoulli's theorem one can then derive an equation for a function $\xi(x,t) = z$ that describes the z-location of the interface between the two phases of the fluid. Details of this calculation can for example be found in Pringle & King (2007). For a single perturbative Fourier mode

$$\xi \;=\; \hat{\xi}\exp[i(kx-\omega t)], \tag{10.99}$$

one then finds that non-trivial solutions with $\hat{\xi} \neq 0$ are possible for

$$\omega^2(\rho_1+\rho_2) - 2\omega k(\rho_1 v_1 + \rho_2 v_2) + k^2(\rho_1 v_1^2 + \rho_2 v_2^2) + (\rho_2-\rho_1)kg = 0, \tag{10.100}$$

which is the *dispersion relation*. Unstable, exponentially growing mode solutions appear if there are solutions for ω with positive imaginary part. Below, we examine the

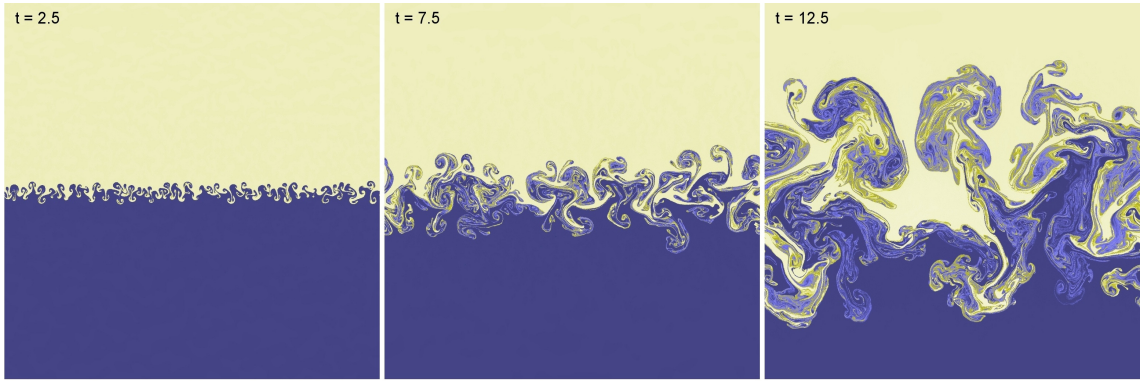

Figure 10.2: A growing Rayleigh-Taylor instability in which a lighter fluid (blue) is covered by a heaver fluid (yellow).

dispersion relation for a few special cases.

10.4.2 Rayleigh-Taylor instability

Let us consider the case of a fluid at rest, $v_1 = v_2 = 0$. The dispersion relation simplifies to

$$\omega^2 = \frac{(\rho_1 - \rho_2)kg}{\rho_1 + \rho_2}. \tag{10.101}$$

We see that for $\rho_2 > \rho_1$, i.e. the denser fluid lies on top, unstable solutions with $\omega^2 < 0$ exist. This is the so-called Rayleigh-Taylor instability. It is in essence buoyancy driven and leads to the rise of lighter material underneath heavier fluid in a stratified atmosphere, as illustrated in the simulation shown in Figure 10.2. The free energy that is tapped here is the potential energy in the gravitational field. Also notice that for an ideal gas, arbitrarily small wavelengths are unstable, and those modes will grow fastest. If on the other hand we have $\rho_1 > \rho_2$, then the interface is stable and will only oscillate when perturbed.

10.4.3 Kelvin-Helmholtz instability

If we set the gravitational field to zero, $g = 0$, we have the situation of a pure shear flow. In this case, the solutions of the dispersion relation are given by

$$\omega_{1/2} = \frac{k(\rho_1 v_1 + \rho_2 v_2)}{\rho_1 + \rho_2} \pm ik\frac{\sqrt{\rho_1 \rho_2}}{\rho_1 + \rho_2}|v_1 - v_2|. \tag{10.102}$$

Interestingly, in an ideal gas there is an imaginary growing mode component for every $|v_1 - v_2| > 0$! This means that a small wave-like perturbation at an interface will

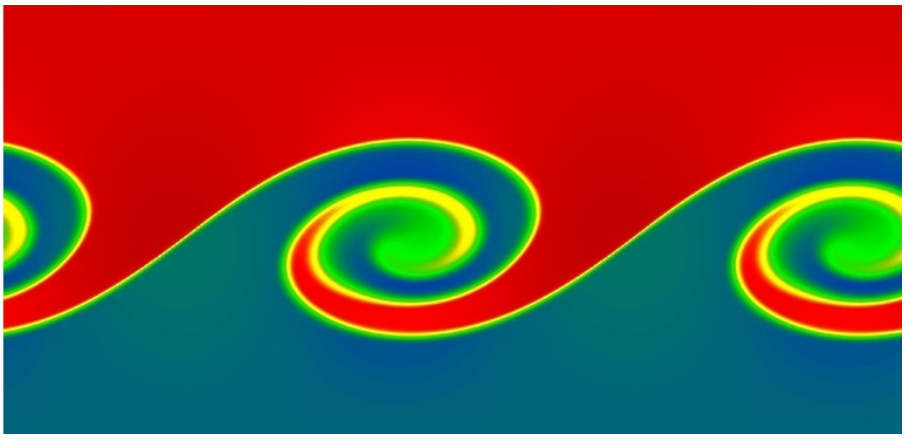

Figure 10.3: Characteristic Kelvin-Helmholtz billows arising in a shear flow.

grow rapidly into large waves that take the form of characteristic Kelvin-Helmholtz "billows". In the non-linear regime reached during the subsequent evolution of this instability the waves are rolled up, leading to the creation of vortex like structures, as seen in Figure 10.3. As the instability grows fastest for small scales (high k), the billows tend to get larger and larger with time.

Because the Kelvin-Helmholtz instability basically means that any sharp velocity gradient in a shear flow is unstable in a freely streaming fluid, this instability is particularly important for the creation of fluid turbulence. Under certain conditions, some modes can however be stabilized against the instability. This happens for example if we consider shearing with $v_1 \neq v_2$ in a gravitational field $g > 0$. Then the dispersion relation has the solutions

$$\omega = \frac{k(\rho_1 v_1 + \rho_2 v_2)}{\rho_1 + \rho_2} \pm \frac{\sqrt{-k^2 \rho_1 \rho_2 (v_1 - v_2)^2 - (\rho_1 + \rho_2)(\rho_2 - \rho_1) k g}}{\rho_1 + \rho_2}. \tag{10.103}$$

Stability is possible if two conditions are met. First, we need $\rho_1 > \rho_2$, i.e. the lighter fluid needs to be on top (otherwise we would have in any case a Rayleigh-Taylor instability). Second, the condition

$$(v_1 - v_2)^2 < \frac{(\rho_1 + \rho_2)(\rho_1 - \rho_2) g}{k \rho_1 \rho_2} \tag{10.104}$$

must be fulfilled. Compared to the ordinary Kelvin-Helmholtz instability without a gravitational field, we hence see that sufficiently small wavenumbers are stabilized below a threshold wavenumber. The larger the shear becomes, the further this threshold moves to small scales.

The Rayleigh-Taylor and Kelvin-Helmholtz instabilities are by no means the only fluid instabilities that can occur in an ideal gas (Pringle & King, 2007). For example, there is also the Richtmyer-Meshkov instability, which can occur when an interface is suddenly

accelerated, for example due to the passage of a shock wave. In self-gravitating gases, there is the Jeans instability, which occurs when the internal gas pressure is not strong enough to prevent a positive density perturbation from growing and collapsing under its own gravitational attraction. This type of instability is particularly important in cosmic structure growth and star formation. If the gas dynamics is coupled to external sources of heat (e.g. through a radiation field), a number of further instabilities are possible. For example, a thermal instability (Field, 1965) can occur when a radiative cooling function has a negative dependence on temperature. If the temperature drops somewhere a bit more through cooling than elsewhere, the cooling rate of this cooler patch will increase such that it is cooling even faster. In this way, cool clouds can drop out of the background gas.

10.5 Turbulence

"Big whirls have little whirls that feed on their velocity,
and little whirls have lesser whirls and so on to viscosity."
– *Lewis Fry Richardson*

Fluid flow which is unsteady, irregular, seemingly random, and chaotic is called *turbulent* (Pope, 2000). Familiar examples of such situations include the smoke from a chimney, a waterfall, or the wind field behind a fast car or airplane. The characteristic feature of turbulence is that the fluid velocity varies significantly and irregularly both in position and time. As a result, turbulence is a statistical phenomenon and is best described with statistical techniques.

If the turbulent motions are subsonic, the flow can often be approximately treated as being incompressible, even for an equation of state that is not particularly stiff. Then only solenoidal motions that are divergence free can occur, or in other words, only shear flows are present. We have already seen that such flows are subject to fluid instabilities such as the Kelvin-Helmholtz instability, which can easily produce swirling motions on many different scales. Such vortex-like motions, also called *eddies*, are the conceptual building blocks of Kolmogorov's theory of incompressible turbulence (Kolmogorov, 1941), which yields a surprisingly accurate description of the basic phenomenology of turbulence, even though many aspects of turbulence are still not fully understood.

10.5.1 Kolmogorov's theory of incompressible turbulence

We start with the Navier-Stokes equation (10.25) for an incompressible fluid, i.e., $\boldsymbol{\nabla} \cdot \boldsymbol{v} = 0$, and obtain

$$\frac{\partial \boldsymbol{v}}{\partial t} + (\boldsymbol{v} \cdot \boldsymbol{\nabla})\boldsymbol{v} = \boldsymbol{g} - \frac{1}{\rho}\boldsymbol{\nabla} P + \nu \Delta \boldsymbol{v}, \tag{10.105}$$

where we used (10.26) and (10.27) and defined the kinematic viscosity $\nu = \eta/\rho = \lambda_{\rm mfp} v_{\rm th}$ which is the product of particle mean free path and thermal velocity and has the units cm^2 s^{-1}. From left to right, the terms have the following meaning: 1) rate of change of $\boldsymbol{v}$, 2) advective transport, 3) external force (e.g., gravity), 4) pressure force, 5) viscous dissipation term.

We compare the time scales for advection, $t_{\rm adv}$, and for viscous dissipation, $t_{\rm diss}$:

$$t_{\rm adv} = \frac{L}{v} \quad \text{and} \quad t_{\rm diss} = \frac{L^2}{\nu}, \tag{10.106}$$

where L and v are characteristic length and velocity scales of the (macroscopic) system. We define the Reynolds number to be the ratio of dissipative-to-advective time scale,

$$\mathrm{Re} = \frac{t_{\rm diss}}{t_{\rm adv}} = \frac{Lv}{\nu} = \frac{L}{\lambda_{\rm mfp}} \frac{v}{v_{\rm th}}. \tag{10.107}$$

This shows that Re is the product of the ratios of macroscopic-to-microscopic length and velocity scales.

Note that the assumption of an incompressible flow

$$\boldsymbol{v}(\boldsymbol{x}, t) = \int \hat{\boldsymbol{v}}(\boldsymbol{k}, \omega) \mathrm{e}^{i(\boldsymbol{k}\cdot\boldsymbol{x} - \omega t)} \mathrm{d}^3 k \mathrm{d}\omega, \tag{10.108}$$

$$\boldsymbol{\nabla} \cdot \boldsymbol{v} = 0 \implies \boldsymbol{k} \cdot \hat{\boldsymbol{v}} = 0 \tag{10.109}$$

does not allow for longitudinal disturbances (sound waves), but only for rotational flows, so-called "eddies" and implies subsonic velocities (since supersonic velocities would cause the formation of shocks, which necessarily have $\boldsymbol{\nabla} \cdot \boldsymbol{v} \neq 0$).

If $\mathrm{Re} \gg 1$, advection is much faster than dissipation which cannot stabilize the dynamical growth. The vortical fluid motions interact non-linearly and turbulence sets in. In three dimensions, energy is being fed into the turbulent cascade on the macroscopic "injection scale" L with a typical velocity v. Energy is being transported from large to small scales as large eddies break up into smaller eddies, thereby conserving vorticity in the absence of the baroclinic term. The energy transport to small scales continues until the energy is dissipated through the production of viscous heat on the microscopic "viscous" scale, $\lambda_{\rm visc}$, which is of order the particle mean free path. The scales in between, for $\lambda_{\rm visc} < \lambda < L$, are called the "inertial range". In two dimensions, however,

small eddies merge to form larger eddies and energy flows from small to large scales along an "inverse cascade".

Let λ be the size of an eddy and v_λ the typical rotational velocity across the eddy. The energy flow through that scale is the product of kinetic energy and the eddy turnover rate on that scale,

$$\epsilon \approx \left(\frac{v_\lambda^2}{2}\right)\left(\frac{v_\lambda}{\lambda}\right) \approx \frac{v_\lambda^3}{\lambda}. \tag{10.110}$$

In the inertial range, the energy flow must be independent on scale, $\epsilon = \text{const.}$ because energy must not accumulate anywhere in steady state: the only channel for the energy to be transferred is through non-linear interactions with other eddies and hence, we obtain the velocity scaling from (10.110)

$$v_\lambda \approx v\left(\frac{\lambda}{L}\right)^{1/3}. \tag{10.111}$$

The largest eddies assume the highest velocities (and thus the highest kinetic energies), but the smallest eddies have the highest vorticity ($\boldsymbol{\omega} = \boldsymbol{\nabla} \times \boldsymbol{v}$)

$$|\boldsymbol{\omega}| \approx \frac{v_\lambda}{\lambda} \approx \frac{v}{(\lambda^2 L)^{1/3}}. \tag{10.112}$$

Since the overall vorticity is approximately conserved this implies that turbulence becomes more and more intermittent on smaller scales, i.e., less volume is filled with turbulent eddies.

10.5.2 Power spectrum of Kolmogorov turbulence

Eddy motions on a length-scale λ correspond to wavenumber $k = 2\pi/\lambda$. The kinetic energy ΔE contained between two wave numbers k_1 and k_2 can be described by

$$\Delta E = \int_{k_1}^{k_2} E(k)\,\mathrm{d}k, \tag{10.113}$$

where $E(k)$ is the so-called energy spectrum. The energy spectrum is related to the three-dimensional velocity power spectrum $P_v(k)$ via

$$E(k)\,\mathrm{d}k = P_v(k)k^2\mathrm{d}k. \tag{10.114}$$

To compute the functional form of this power spectrum, we write down the correlation function

$$\xi_v(y) \equiv \langle \boldsymbol{v}(\boldsymbol{x}) \cdot \boldsymbol{v}(\boldsymbol{x}+\boldsymbol{y})\rangle, \tag{10.115}$$

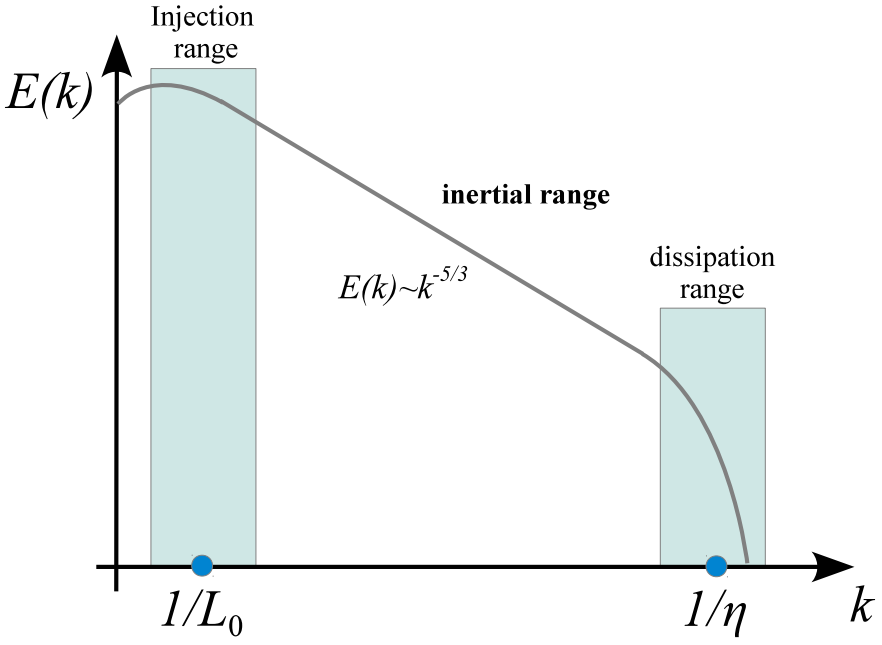

Figure 10.4: Schematic energy spectrum of Kolmogorov turbulence.

which does not depend on the direction of $\boldsymbol{y}$ since turbulence is statistically isotropic. Noting that the eddy velocity, $v_\lambda \approx (\epsilon\lambda)^{1/3}$, we find that the correlation function scales as

$$\xi_v \propto v_\lambda^2 \propto (\epsilon\lambda)^{2/3}. \tag{10.116}$$

Interestingly, the kinetic energy on a scale λ scales exactly as the correlation function, $e_\lambda \propto v_\lambda^2 \propto \lambda^{2/3}$. As shown in Appendix **??**, correlation functions and power spectra are related by a Fourier transformation. Hence, the velocity power spectrum inherits the scaling of correlation function ξ_v,

$$P_v(k) \propto \lambda^3 \xi_v \propto k^{-3} \left(\epsilon k^{-1}\right)^{2/3} \propto \epsilon^{2/3} k^{-11/3}. \tag{10.117}$$

Accounting for the volume element in wave number space, the power per linear and logarithmic interval in k-space are given by

$$P_v(k)k^2\mathrm{d}k = C\epsilon^{2/3}k^{-5/3}\mathrm{d}k, \quad \text{and} \tag{10.118}$$

$$P_v(k)k^3\mathrm{d}\ln k = C\epsilon^{2/3}k^{-2/3}\mathrm{d}\ln k, \tag{10.119}$$

which is the Kolmogorov turbulence spectrum of driven turbulence. The constant C is universal in Kolmogorov's theory, but cannot be computed from first principles. Experiment and numerical simulations give $C \simeq 1.5$ (Pope, 2000).

Actually, if we recall Kolmogorov's first similarity hypothesis, it makes the stronger claim that the statistics for all small scale motion is universal. This means that also the dissipation part of the turbulence must have a universal form. To include this in the description of the spectrum, we can for example write for the energy spectrum

$$E(k) \equiv P_v(k)k^2 = C\,\epsilon^{2/3}\,k^{-5/3} f_\eta(k\eta), \tag{10.120}$$

where $f_\eta(k\eta)$ us a universal function with $f_\eta(x) = 1$ for $x \ll 1$, and with $f_\eta(x) \to 0$ for $x \to \infty$. This function has to be determined experimentally or numerically. A good fit to different results is given by

$$f_\eta(x) = \exp\left(-\beta[(x^4 + c^4)^{1/4} - c]\right), \tag{10.121}$$

with $\beta_0 \sim 5.2$ and $c \sim 0.4$ (Pope, 2000).

11 Eulerian hydrodynamics

Many physical theories are expressed as partial differential equations (PDEs), including some of the most fundamental laws of nature, such as fluid dynamics (Euler and Navier Stokes equations), electromagnetism (Maxwell's equations) or general relativity/gravity (Einstein's field equations). Broadly speaking, partial differential equations (PDE) are equations describing relations between partial derivatives of a dependent variable with respect to several independent variables. For example,

$$\frac{\partial u}{\partial t} = \frac{\partial^2 u}{\partial x^2} \tag{11.1}$$

is a PDE for the function $u = u(x, t)$. The independent variables are here x and t, the dependent variable is u (i.e. the function value). Unlike for ordinary differential equations (ODEs), there is no simple unified theory for PDEs. Rather, there are different types of PDEs which exhibit special features.

Given that the fundamental laws of classical physics are expressed in terms of partial differential equations, it is clear that such equations are of fundamental importance in all of physics. The solutions of PDEs can be extremely complex, encoding many physical phenomena. Simulation techniques are crucial to uncover and understand parts of the solution spaces of PDEs. But depending on the PDEs, numerically solving them can be very tricky, and is quite generally more difficult than solving systems of ordinary differential equations.

11.1 Types of PDEs

It is useful to distinguish different properties of PDEs in order to help classifying them. Some of the most important characteristics include:

- **Order of the PDE:** This is simply the highest derivative appearing in the PDE. A "second-order PDE" will have up to second partial derivatives.
- **Linearity:** A PDE (or system of PDEs) is linear if all terms are linear in the unknown function (the dependent variable) and its partial derivatives. Linear PDEs are (unsurprisingly) much simpler to solve than non-linear ones.

- **Homogeneity:** If all its terms contain the dependent (unknown) variable or its derivative, the PDE is said to be homogeneous. Otherwise it contains "source-terms" and is inhomogeneous.

In addition, PDEs can be classified according to some less obvious features which are however reflecting the nature of the physics that the PDEs describe. For example, the hydrodynamic fluid equations are local conservation laws, hence they are expressed as so-called *hyperbolic* conservation laws. What this means will be discussed later in more detail.

The most important linear and homogeneous PDEs

In order to introduce the different characters of PDEs, let us look at the **three most important linear and homogeneous PDEs**. These arguably are:

1. Laplace equation:
$$\frac{\partial^2 u}{\partial x^2} + \frac{\partial^2 u}{\partial y^2} + \frac{\partial^2 u}{\partial z^2} = 0 \tag{11.2}$$

2. Heat conduction equation
$$\frac{\partial u}{\partial t} = \lambda^2 \left(\frac{\partial^2 u}{\partial x^2} + \frac{\partial^2 u}{\partial y^2} + \frac{\partial^2 u}{\partial z^2} \right) \tag{11.3}$$

3. Wave equation
$$\frac{\partial^2 u}{\partial t^2} = c^2 \left(\frac{\partial^2 u}{\partial x^2} + \frac{\partial^2 u}{\partial y^2} + \frac{\partial^2 u}{\partial z^2} \right) \tag{11.4}$$

These equations look quite similar, but their type and character is fundamentally different. In fact, one needs different techniques for solving them. One thing they have in common however is that, thanks to their linearity, if u_1 and u_2 are two solutions, then all linear combinations $c_1 u_1 + c_2 u_2$ are also solutions, which is the superposition principle.

Often, PDEs are characterized in terms of properties that are called

- elliptic
- parabolic
- hyperbolic

We now discuss how this general characterization of the PDE-type is defined. For linear 2nd-order PDEs of the form (a, b, c not all zero)
$$a\frac{\partial^2 u}{\partial x^2} + b\frac{\partial^2 u}{\partial x \partial y} + c\frac{\partial^2 u}{\partial y^2} + d\frac{\partial u}{\partial x} + e\frac{\partial u}{\partial y} + f\, u = g. \tag{11.5}$$

We proceed by expanding the unknown function into plane waves (i.e., a Fourier transformation):

$$u(\boldsymbol{x}) = \int \frac{\mathrm{d}^2 k}{(2\pi)^2}\, \hat{u}(\boldsymbol{k}) \mathrm{e}^{-i\boldsymbol{k}\cdot\boldsymbol{x}}\,, \quad \text{where } \boldsymbol{k} = (k, l), \tag{11.6}$$

and obtain the following equation

$$-\int \frac{\mathrm{d}^2 k}{(2\pi)^2}\, \left(ak^2 + bkl + cl^2 + idk + iel - f\right) \hat{u}(\boldsymbol{k}) \mathrm{e}^{-i\boldsymbol{k}\cdot\boldsymbol{x}} = g. \tag{11.7}$$

First, we separate the homogeneous equation from the source term of the right-hand side. A solution requires the parenthesis to vanish identically. The parenthesis can be written in matrix notation

$$\begin{pmatrix} k & l \end{pmatrix} \begin{pmatrix} a & b/2 \\ b/2 & c \end{pmatrix} \begin{pmatrix} k \\ l \end{pmatrix} + i \begin{pmatrix} d & e \end{pmatrix} \begin{pmatrix} k \\ l \end{pmatrix} - f = 0. \tag{11.8}$$

This equation describes conic sections (Fig. 11.1). Hence, solutions of this equation are classified in terms of the discriminant

$$D = -4\Delta = b^2 - 4ac, \quad \text{where } \Delta = \begin{vmatrix} a & b/2 \\ b/2 & c \end{vmatrix} \tag{11.9}$$

is the matrix determinant. The following cases are distinguished:

$$D \begin{cases} < 0 & \text{elliptic,} \\ = 0 & \text{parabolic,} \\ > 0 & \text{hyperbolic.} \end{cases} \tag{11.10}$$

PDEs that fall in the same class of these types often exhibit similar mathematical and physical properties, and also require similar solution strategies.

Examples for types of 2nd-order PDEs:

Let's go back to our 'three most important PDEs' from above and consider only two independent variables for now.

1. For the Laplace equation we have:

$$\frac{\partial^2 u}{\partial x^2} + \frac{\partial^2 u}{\partial y^2} = 0, \tag{11.11}$$

   So here, we can identify $a = 1$, $b = 0$, and $c = 1$. Therefore $D = -4 < 0$, and the equation is *elliptic*.

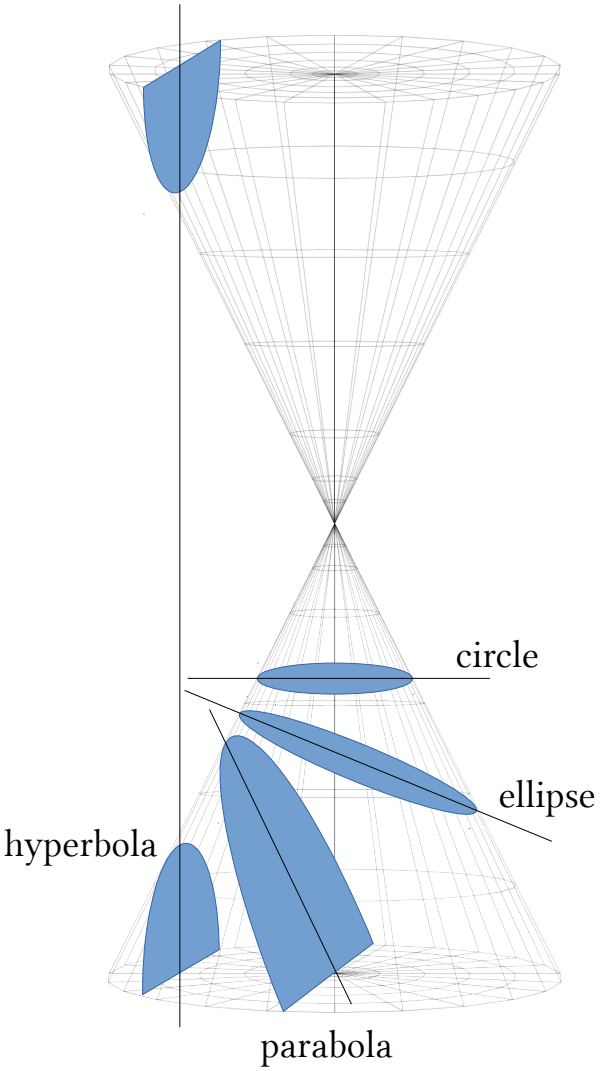

Figure 11.1: This figure describes the conic sections circle, ellipse, parabola and hyperbola, depending on the location of the sectional cut plane.

2. The heat conduction equation takes the form:

$$\frac{\partial u}{\partial t} - \lambda^2 \frac{\partial^2 u}{\partial x^2} = 0. \tag{11.12}$$

   Here we have $a = 0$, $b = 0$ and $c = -\lambda^2$, hence $D = 0$. This is a *parabolic* equation.

3. Finally, the wave equation is

$$\frac{\partial^2 u}{\partial t^2} - c_s^2 \frac{\partial^2 u}{\partial x^2} = 0. \tag{11.13}$$

   yielding $a = 1$, $b = 0$ and $c = -c_s^2$. Hence $D = 4c_s^2 > 0$ and this equation is therefore *hyperbolic*.

General linear PDEs of 2nd-order with more unknowns than two can be written as

$$\sum_{i,j=1}^{n} a_{ij} \frac{\partial^2 u}{\partial x_i \partial x_j} + \sum_i b_i \frac{\partial u}{\partial x_i} + cu + d = 0. \tag{11.14}$$

Here the eigenvalues of the coefficient matrix a_{ij} can be used to determine the type, according to the following scheme:

- elliptic: all eigenvalues positive, or all negative
- parabolic: one zero eigenvalue, the others all positive or all negative
- hyperbolic: one negative eigenvalue the rest all positive, or one positive the rest all negative

Other cases (multiple eigenvalues of different sign) are sometimes called ultra-hyperbolic. Note that in 2D, this definition should be the same as our previous one. We can readily check that. To make contact with the previous notation, the coefficient matrix is then

$$a_{ij} = \begin{pmatrix} a & b/2 \\ b/2 & c \end{pmatrix}. \tag{11.15}$$

The characteristic equation for the eigenvalues has solutions

$$\lambda_{1,2} = \frac{(a+c) \pm \sqrt{(a+c)^2 - 4ac + b^2}}{2}. \tag{11.16}$$

We can again distinguish the three cases from above:

1. For $b = 0$, the eigenvalues are $\lambda_{1,2} = \{a, c\}$. Hence, if $ac > 0$ we have $D = -4ac < 0$, and we have an *elliptic* equation if and only if the two eigenvalues are both positive or both negative.
2. For a *parabolic* equation, we have $D = 0$ or equivalently, $4ac = b^2$. Thus, we obtain the eigenvalues $\lambda_{1,2} = \{a + c, 0\}$, i.e., one zero eigenvalue and one non-zero eigenvalue.
3. Finally, we have two real eigenvalues with opposite signs if $D = b^2 - 4ac > 0$, which corresponds to the *hyperbolic* case, consistent with our previous simpler definition.

Linear systems of first-order PDEs

Linear systems of first-order homogeneous PDEs can be written as

$$\frac{\partial u_i}{\partial t} + \sum_j A_{ij} \frac{\partial u_i}{\partial x_j} = 0, \tag{11.17}$$

where $\mathbf{A} = (A_{ij})$ is a coefficient matrix, and one independent variable has been singled out as 'time' t. We may also use a more compact notation of the form

$$\frac{\partial \boldsymbol{u}}{\partial t} + \mathbf{A} \cdot \frac{\partial \boldsymbol{u}}{\partial \boldsymbol{x}} = \mathbf{0} \tag{11.18}$$

for this. Here, if $\mathbf{A}$ has only *real eigenvalues* and is diagonalizable, then the PDE system is called *hyperbolic* as well.

This definition can also be extended to non-linear PDEs of the form

$$\frac{\partial \boldsymbol{u}}{\partial t} + \frac{\partial}{\partial \boldsymbol{x}} \cdot \mathbf{F}(\boldsymbol{u}) = \mathbf{0}, \tag{11.19}$$

where $\mathbf{F}(\boldsymbol{u})$ is a matrix that may depend on $\boldsymbol{u}$. Such PDEs are called conservation laws, where $\boldsymbol{u}$ are conserved variables and $\mathbf{F}$ is the flux (compare with the continuity equation). One can also write this equation in quasi-linear form by invoking the chain rule:

$$\frac{\partial \boldsymbol{u}}{\partial t} + \frac{\partial \mathbf{F}}{\partial \boldsymbol{u}} \cdot \frac{\partial \boldsymbol{u}}{\partial \boldsymbol{x}} = \mathbf{0}, \tag{11.20}$$

or more compactly as

$$\frac{\partial \boldsymbol{u}}{\partial t} + \overline{\mathbf{A}} \cdot \frac{\partial \boldsymbol{u}}{\partial \boldsymbol{x}} = \mathbf{0}, \tag{11.21}$$

where $\overline{\mathbf{A}} = \partial \mathbf{F} / \partial \boldsymbol{u}$ is the Jacobian of the flux. Now, if $\overline{\mathbf{A}}$ is diagonalizable and has real eigenvalues, we still call the (non-linear) set of equations a hyperbolic PDE system.

Character and boundary conditions of different PDE types

The different classes of PDEs show qualitatively different behavior in their solutions. Broadly speaking, the following observations can be made:

- **Elliptic PDEs** often describe static problems without time dependence, or equilibrium states of some kind. An important example is the Poisson equation for the gravitational or electrostatic field. The solutions of elliptic problems tend to be as smooth as allowed by the boundary conditions and source terms.
- **Parabolic PDEs** are often of second-order and describe slowly changing processes (for example diffusion). Solutions become here *smoother* with time. For describing the problem, one needs the initial state $u(x, t_0)$ as well as boundary conditions.
- **Hyperbolic PDEs in physics** typically describe dynamical processes of systems that start with some known initial conditions at time t_0. Solutions can develop steep regions or real discontinuities with time, even if they start with perfectly smooth initial states. To specify the initial conditions completely, one needs $u(x, t_0)$ and $\frac{\partial u}{\partial x}(x, t_0)$ and higher derivatives if present, as well as boundary conditions.

For all types of PDEs, boundary conditions are very important and need to be specified to determine the solution uniquely. If the value of the sought function is specified with a fixed value on the boundaries, one calls this *Dirichlet* boundary conditions. If instead the value of the derivative of u is prescribed on the boundary (usually in the normal direction with respect to the boundary), one has so-called *von Neumann* boundary conditions.

11.2 Solution schemes for PDEs

Unfortunately, for partial differential equations one cannot give a general solution method that works equally well for all types of problems. Rather, each type requires different approaches, and certain PDEs encountered in practice may even be best addressed with special custom techniques built by combining different elements from standard techniques. Important classes of solution schemes include the following:

- **Finite difference methods:** Here the differential operators are approximated through finite difference approximations, usually on a regular (Cartesian) mesh, or some other kind of structured mesh (for example a polar grid). An example we already previously discussed is Poisson's equation treated with iterative (multigrid) methods.
- **Finite volume methods:** These may be seen as a subclass of finite difference methods. They are particularly useful for hyperbolic conservation laws. We shall discuss examples for this approach in applications to fluid dynamics later in this section.
- **Spectral methods:** Here the solution is represented by a linear combination of functions, allowing the PDE to be transformed to algebraic equations or ordinary differential equations. Often this is done by applying Fourier techniques. For example, solving the Poisson equation with FFTs, as we discussed earlier, is a spectral method.
- **Method of lines:** This is a semi-discrete approach where all derivatives except for one are approximated with finite differences. The remaining derivative is then the only one left, so that the remaining problem forms a set of ordinary differential equations (ODEs). Very often, this approach is used in time-dependent problems. One here discretizes space in terms of a set of N points x_i, and for each of these points one obtains an ODE that describes the time evolution of the function at this point. The PDE is transformed in this way into a set of N coupled ODEs. For example, consider the heat diffusion equation in one dimension,

$$\frac{\partial u}{\partial t} + \lambda \frac{\partial^2 u}{\partial x^2} = 0. \tag{11.22}$$

If we discretize this into a set of points that are spaced h apart, we obtain N equations

$$\frac{\mathrm{d}u_i}{\mathrm{d}t} + \lambda \frac{u_{i+1} + u_{i-1} - 2u_i}{h^2} = 0. \tag{11.23}$$

These differential equations can now be integrated in time as an ODE system. Note however that this is not necessarily stable. Some problems may require upwinding, i.e. asymmetric forms for the finite difference estimates to recover stability.

- **Finite element methods:** Here the domain is subdivided into "cells" (elements) of fairly arbitrary shape. The solution is then represented in terms of simple, usually polynomial functions on the element, and then the PDE is transformed to an algebraic problem for the coefficients in front of these simple functions. This is hence similar in spirit to spectral methods, except that the expansion is done in terms of highly localized functions on an element by element basis, and is truncated already at low order.

In practice, many different variants of these basic methods exist, and sometimes also combinations of them are used.

11.3 Simple advection

First-order equations of hyperbolic type are particularly useful for introducing the numerical difficulties that then also need to be addressed for more complicated non-linear conservation laws (e.g. Toro, 1997; LeVeque, 2002; Stone et al., 2008). The simplest equation of this type is the *advection equation* in one dimension. This is given by

$$\frac{\partial u}{\partial t} + v \frac{\partial u}{\partial x} = 0, \tag{11.24}$$

where $u = u(x, t)$ is a function of x and t, and v is a constant parameter. This equation is hyperbolic because the so-called coefficient matrix[1] is real and trivially diagonalizable.

If we are given any function $q(x)$, then

$$u(x, t) = q(x - vt) \tag{11.26}$$

is a solution of the PDE, as one can easily check. We can interpret $u(x, t = 0) = q(x)$ as initial condition, and the solution at a later time is then an exact copy of q, simply translated by $v\,t$ along the x-direction, as shown in Fig. 11.2.

[1] A linear system of first-order PDEs can be written in the generic form

$$\frac{\partial u_i}{\partial t} + \sum_j A_{ij} \frac{\partial u_i}{\partial x_j} = 0, \tag{11.25}$$

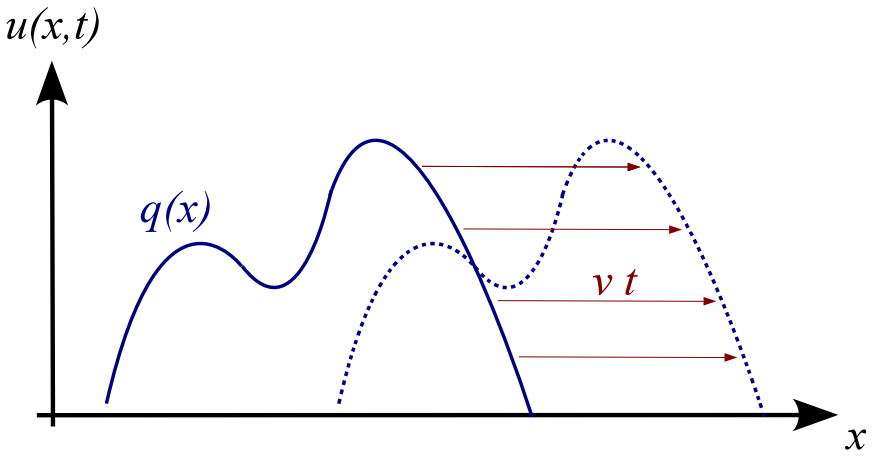

Figure 11.2: Simple advection with constant velocity to the right.

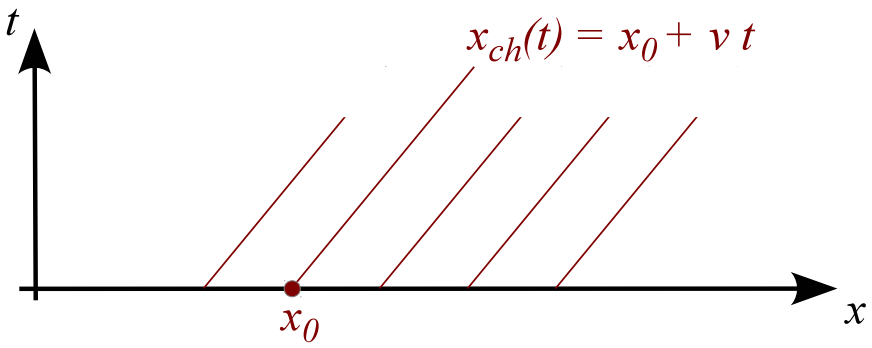

Figure 11.3: A set of flow characteristics for advection to the right with constant velocity v.

Points that start at a certain coordinate x_0 are advected to a new location $x_{\rm ch}(t) = vt + x_0$. These so-called *characteristics* (see Fig. 11.3), which can be viewed as mediating the propagation of information in the system, are straight lines, all oriented in the downstream direction. Note that "downstream" refers to the direction in which the flow goes, whereas "upstream" is from where the flow comes.

Let's now assume we want to solve the advection problem numerically. (Strictly speaking this is of course superfluous as we have an analytic solution in this case, but we want to see how well a numerical technique would perform here.) We can approach this with a straightforward discretization of u on a spatial mesh, using for example the method of lines. This gives us:

$$\frac{{\rm d}u_i}{{\rm d}t} + v\frac{u_{i+1} - u_{i-1}}{2h} = 0. \tag{11.27}$$

where A_{ij} is the coefficient matrix.

If we go one step further and also discretize the time derivative with a simple Euler scheme, we get

$$u_i^{(n+1)} = u_i^{(n)} - v\frac{u_{i+1}^{(n)} - u_{i-1}^{(n)}}{2h}\Delta t. \tag{11.28}$$

This is a complete update formula which can be readily applied to a given initial state on the grid. The big surprise is that this turns out to be quite violently unstable! For example, if one applies this to the advection of a step function, one invariably obtains strong oscillatory errors in the downstream region of the step, quickly rendering the numerical solution into complete garbage. What is the reason for this fundamental failure?

- First note that all characteristics (signals) propagate downstream in this problem, or in other words, information strictly travels in the flow direction in this problem.
- But, the information to update u_i is derived both from the upstream (u_{i-1}) and the downstream (u_{i+1}) sides.
- According to how the information flows, u_i should not really depend on the downstream side at all, which in some sense is causally disconnected. So let's try to eliminate this dependence by going to a one-sided approximation for the spatial derivative, of the form:

  $$\frac{\mathrm{d}u_i}{\mathrm{d}t} + v\frac{u_i - u_{i-1}}{h} = 0. \tag{11.29}$$

  This is called *upwind differencing*. Interestingly, now the stability problems are completely gone since we only use information from the direction of the wind/stream that can influence the solution in cell i!
- But there are still some caveats to observe: First of all, the discretization now depends on the sign of v. For negative v, one instead has to use

  $$\frac{\mathrm{d}u_i}{\mathrm{d}t} + v\frac{u_{i+1} - u_i}{h} = 0. \tag{11.30}$$

  The other is that the solution is not advected in a perfectly faithful way, instead it is quite significantly smoothed out, through a process one calls *numerical diffusion*.

We can actually understand where this strong diffusion in the 1st-order upwind scheme comes from. To this end, let's rewrite the upwind finite difference approximation of the spatial derivative as

$$\frac{u_i - u_{i-1}}{h} = \frac{u_{i+1} - u_{i-1}}{2h} - \frac{u_{i+1} - 2u_i + u_{i-1}}{2h}. \tag{11.31}$$

Hence our stable upwind scheme can also be written as

$$\frac{\mathrm{d}u_i}{\mathrm{d}t} + v\frac{u_{i+1} - u_{i-1}}{2h} = \frac{vh}{2}\,\frac{u_{i+1} - 2u_i + u_{i-1}}{h^2}. \tag{11.32}$$

But recal that the numerical disretization of the second derivative is given by

$$\left(\frac{\partial^2 u}{\partial x^2}\right)_i \simeq \frac{\partial}{\partial x}\left(\frac{u_{i+1/2}-u_{i-1/2}}{h}\right) \simeq \frac{1}{h}\left(\frac{u_{i+1}-u_i}{h}-\frac{u_i-u_{i-1}}{h}\right) = \frac{u_{i+1}-2u_i+u_{i-1}}{h^2}, \tag{11.33}$$

where we have iteratively used the central differencing formula for the spatial derivatives. If we define a diffusion constant $D = vh/2$, we are effectively solving the following problem,

$$\frac{\partial u}{\partial t} + v\frac{\partial u}{\partial x} = D\frac{\partial^2 u}{\partial x^2}, \tag{11.34}$$

and not the original advection problem. The diffusion term on the right hand side is here a byproduct of the numerical algorithm that we have used. We needed to add this numerical diffusion in order to obtain stability of the integration.

Note however that for better grid resolution, $h \to 0$, the diffusion becomes smaller, so in this limit one obtains an ever better solution. Also note that the diffusivity becomes larger for larger velocity v, so the faster one needs to advect, the stronger the numerical diffusion effects become.

Besides the upwinding requirement, integrating a hyperbolic conservation law with an explicit method in time also requires the use of a sufficiently small integration timestep, not only to get sufficiently good accuracy, but also for reasons of *stability*. In essence, there is a maximum timestep that may be used before the integration brakes down. How large can we make this timestep? Again, we can think about this in terms of information travel. If the timestep exceeds $\Delta t_{\max} = h/v$, then the updating of u_i would have to include information from u_{i-2}, but if we don't do this, the updating will likely become unstable.

This leads to the so-called *Courant-Friedrichs-Levy* (CFL) timestep condition (Courant et al., 1928), which for this problem takes the form

$$\Delta t \leq \frac{h}{v}. \tag{11.35}$$

This is a necessary but not sufficient condition for any explicit finite difference approach of the hyperbolic advection equation. For other hyperbolic conservation laws, similar CFL-conditions apply.

Hyperbolic conservation laws

We now consider a hyperbolic conservation law, such as the continuity equation for the mass density of a fluid:

$$\frac{\partial \rho}{\partial t} + \boldsymbol{\nabla} \cdot (\rho \boldsymbol{v}) = 0. \tag{11.36}$$

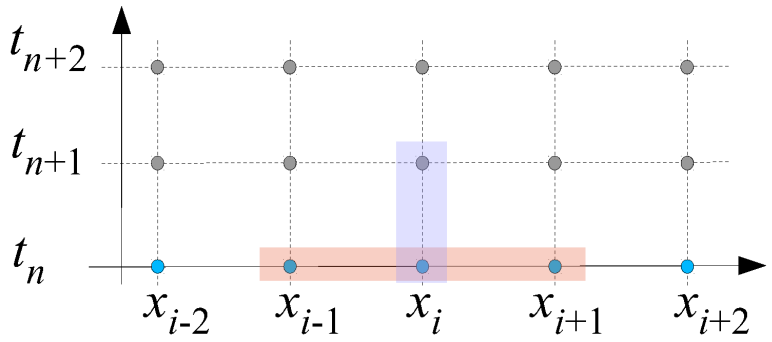

Figure 11.4: A discretization scheme for the continuity equation in one spatial dimension. The red and blue boxes mark the stencils that are applied for calculating the spatial and time derivatives.

We see that this is effectively the advection equation, but with a spatially variable velocity $\boldsymbol{v} = \boldsymbol{v}(\boldsymbol{x})$. Here $\boldsymbol{F} = \rho\boldsymbol{v}$ is the mass flux.

Let's study the problem in one spatial dimension, and consider a discretization both of the x- and t-axis. This corresponds to

$$\frac{\rho_i^{(n+1)} - \rho_i^{(n)}}{\Delta t} + \frac{F_{i+1}^{(n)} - F_{i-1}^{(n)}}{2\Delta x} = 0, \tag{11.37}$$

leading to the update rule

$$\rho_i^{(n+1)} = \rho_i^{(n)} + \frac{\Delta t}{2\Delta x}\left(F_{i-1}^{(n)} - F_{i+1}^{(n)}\right). \tag{11.38}$$

This is again found to be highly unstable, for the same reasons as in the plain advection problem: we have not observed in 'which direction the wind blows', or in other words, we have ignored in which direction the local characteristics point. For example, if the mass flux is to the right, we know that the characteristics point also to the right. The upwind direction is therefore towards negative x, and by using only this information in making our spatial derivative one-sided, we should be able to resurrect stability.

Now, for the mass continuity equation identifying the local characteristics is quite easy, and in fact, their direction can simply be inferred from the sign of the mass flux. However, in more general situations for systems of non-linear PDEs, this is far less obvious. Here we need to use a so-called Riemann solvers to give us information about the local solution and the local characteristics (Toro, 1997). This then also implicitly identifies the proper upwinding that is needed for stability.

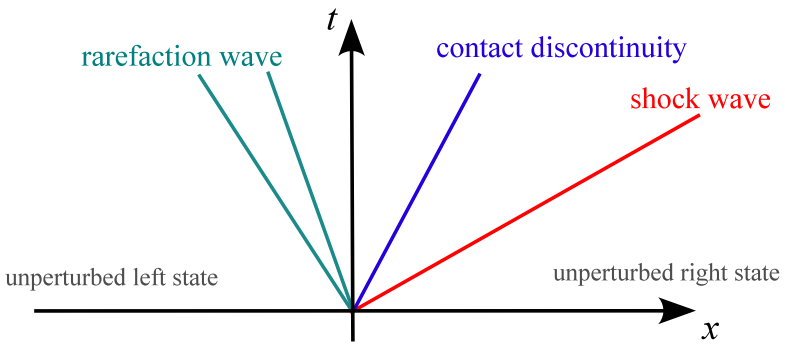

Figure 11.5: Wave structure of the solution of the Riemann problem. The central contact wave separates the original fluid phases. On the left and the right, there is either a shock or a rarefaction wave.

11.4 Riemann problem

The Riemann problem is an initial value problem for a hyperbolic system, consisting of two piece-wise constant states (two half-spaces) that meet at a plane at $t = 0$. The task is then to solve for the subsequent evolution at $t > 0$.

An important special case is the Riemann problem for the Euler equations (i.e. for ideal gas dynamics). Here the left and right states of the interface, can, for example, be uniquely specified by giving the three "primitive" variables density, pressure and velocity, viz.

$$U_L = \begin{pmatrix} \rho_L \\ P_L \\ \boldsymbol{v}_L \end{pmatrix}, \quad U_R = \begin{pmatrix} \rho_R \\ P_R \\ \boldsymbol{v}_R \end{pmatrix}. \tag{11.39}$$

Alternatively one can also specify density, momentum density, and energy density. For an ideal gas, this initial value problem can be solved analytically (Toro, 1997), modulo an implicit equation which requires numerical root-finding, i.e. the solution cannot be written down explicitly. The solution always contains characteristics for three self-similar waves, as shown schematically in Fig. 11.5. Some notes on this:

- The middle wave is always present and is a contact wave that marks the boundary between the original fluid phases from the left and right sides.
- The contact wave is sandwiched between a shock or a rarefaction wave on either side (it is possible to have shocks on both sides, or rarefactions on both sides, or one of each). The rarefaction wave is not a single characteristic but rather a rarefaction fan with a beginning and an end.
- These waves (shock, contact discontinuity, rarefaction) propagate with constant speed. If the solution is known at some time $t > 0$, it can also be obtained at

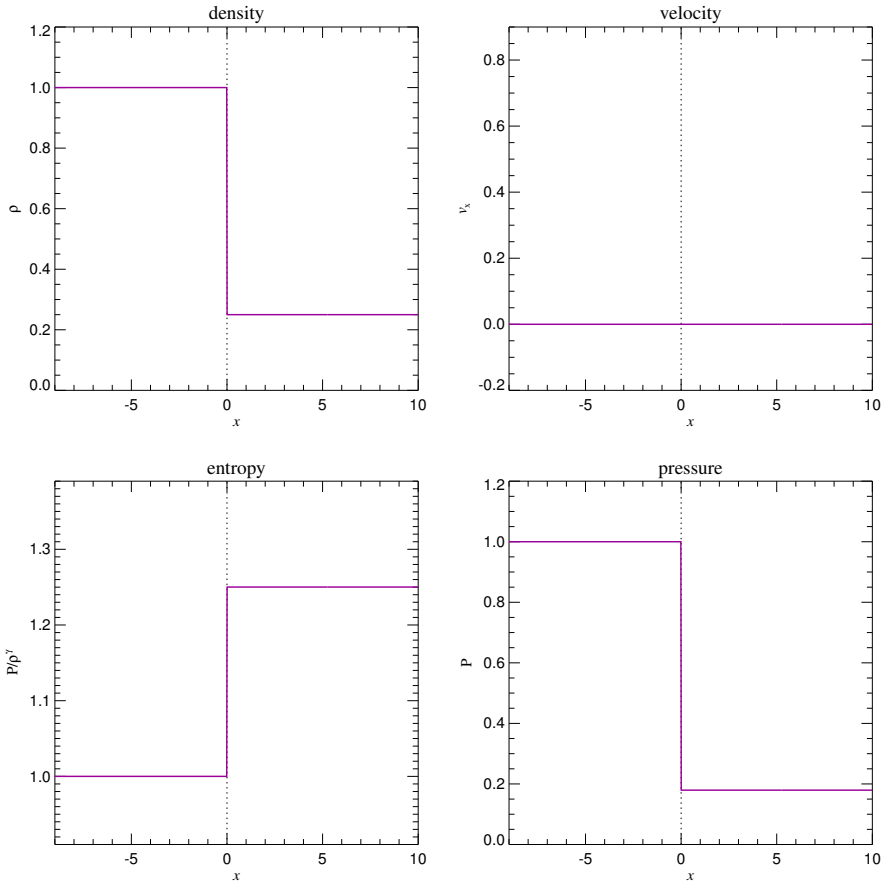

Figure 11.6: Initial state of an example Riemann problem, composed of two phases in different states that are brought into contact at $x = 0$ at time $t = 0$. (Since $v_x = 0$, the initial conditions are actually an example of the special case of a Sod shock-tube problem.)

any other time through a suitable scaling transformation. An important corollary is that at $x = 0$, the fluid quantities in the region that contains the interface $(\rho^\star, P^\star, \boldsymbol{v}^\star)$ are *constant in time* for $t > 0$.

- For $\boldsymbol{v}_L = \boldsymbol{v}_R = 0$, the Riemann problem simplifies and becomes the 'Sod shock tube' problem.

Let's consider an example how this wave structure looks in a real Riemann problem. We consider, for definiteness, a Riemann problem with $\rho_L = 1.0$, $P_L = 1.0$, $v_L = 0$, and $\rho_R = 0.25$, $P_R = 0.1795$, $v_R = 0$ (which is of Sod-shock type). The adiabatic exponent is taken to be $\gamma = 1.4$. We hence deal at $t = 0.0$ with the initial state displayed in Figure 11.6. After time $t = 5.0$, the wave structure formed by a rarefaction to the left (location marked in green), a contact in the middle (blue) and a shock to the right (red) can be nicely seen in Figure 11.7.

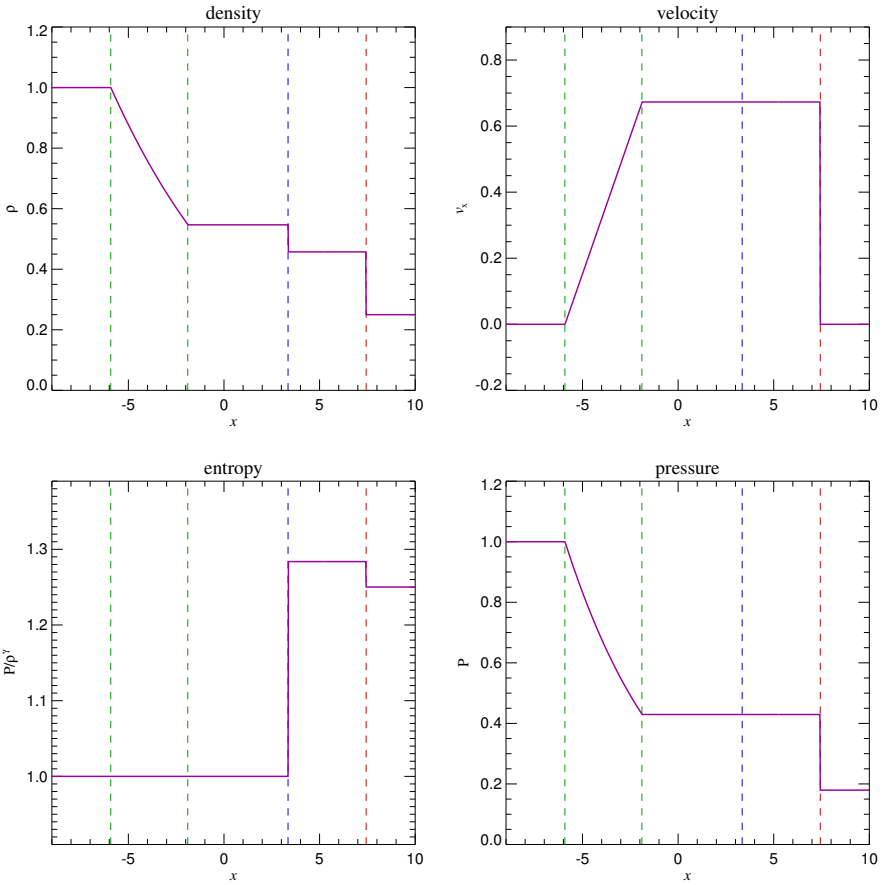

Figure 11.7: Evolved state at $t = 5.0$ of the initial fluid state displayed in Fig. 11.6. The blue dashed line marks the position of the contact wave, the green dashed lines give the location of the rarefaction fan, and the red dashed line marks the shock.

Some general properties of the waves appearing in the Riemann problem can be summarized as follows:

- *Shock:* This is a sudden compression of the fluid, associated with an irreversible conversion of kinetic energy to heat, i.e. here entropy is produced. The density, normal velocity component, pressure, and entropy all change discontinuously at a shock.
- *Contact discontinuity:* This traces the original separating plane between the two fluid phases that have been brought into contact. Pressure as well as the normal velocity are constant across a contact, but density, entropy and temperature can jump.
- *Rarefaction wave:* This occurs when the gas (suddenly) expands. The rarefaction wave smoothly connects two states over a finite spatial region; there are no discontinuities in any of the fluid variables.

11.5 Finite volume discretization

Let's now take a look how Riemann solvers can be used in the finite volume discretization approach to the PDEs of fluid dynamics. Recall that we can write our hyperbolic conservation laws as

$$\frac{\partial \boldsymbol{U}}{\partial t} + \boldsymbol{\nabla} \cdot \mathbf{F} = \mathbf{0}. \tag{11.40}$$

Here $\boldsymbol{U}$ is a state vector and $\mathbf{F}$ is the flux matrix. For example, the Euler equations of section 10.2.1 can be written in the form

$$\boldsymbol{U} = \begin{pmatrix} \rho \\ \rho \boldsymbol{v} \\ \rho e \end{pmatrix}, \qquad \mathbf{F} = \begin{pmatrix} \rho \boldsymbol{v} \\ \rho \boldsymbol{v}\boldsymbol{v}^T + P\mathbf{1} \\ (\rho e + P)\boldsymbol{v} \end{pmatrix}, \tag{11.41}$$

with the specific energy $e = e_{\text{th}} + \boldsymbol{v}^2/2$ and e_{th} being the thermal energy per unit mass. The ideal gas equation gives the pressure as $P = (\gamma - 1)\rho e_{\text{th}}$ and provides a closure for the system.

In a finite volume scheme, we describe the system through the averaged state over a set of finite cells. These cell averages are defined as

$$\boldsymbol{U}_i = \frac{1}{V_i} \int_{\text{cell } i} \boldsymbol{U}(\boldsymbol{x}) \, \mathrm{d}V. \tag{11.42}$$

Let's now see how we could devise an update scheme for these cell-averaged quantities in one dimension for simplicity.

1. We start by integrating the conservation law over a cell, and over a finite interval in time (and replacing the flux matrix by the flux vector $\boldsymbol{F}$):

$$\int_{x_{i-\frac{1}{2}}}^{x_{i+\frac{1}{2}}} \mathrm{d}x \int_{t_n}^{t_{n+1}} \mathrm{d}t \left(\frac{\partial \boldsymbol{U}}{\partial t} + \frac{\partial \boldsymbol{F}}{\partial x} \right) = 0. \tag{11.43}$$

2. This gives

$$\int_{x_{i-\frac{1}{2}}}^{x_{i+\frac{1}{2}}} \mathrm{d}x \left[\boldsymbol{U}(x, t_{n+1}) - \boldsymbol{U}(x, t_n) \right] + \int_{t_n}^{t_{n+1}} \mathrm{d}t \left[\boldsymbol{F}(x_{i+\frac{1}{2}}, t) - \boldsymbol{F}(x_{i-\frac{1}{2}}, t) \right] = 0. \tag{11.44}$$

   In the first term, we recognize the definition of the cell average:

$$\boldsymbol{U}_i^{(n)} \equiv \frac{1}{\Delta x} \int_{x_{i-\frac{1}{2}}}^{x_{i+\frac{1}{2}}} \boldsymbol{U}(x, t_n) \mathrm{d}x. \tag{11.45}$$

   Hence we have

$$\Delta x \left[\boldsymbol{U}_i^{(n+1)} - \boldsymbol{U}_i^{(n)} \right] + \int_{t_n}^{t_{n+1}} \mathrm{d}t \left[\boldsymbol{F}(x_{i+\frac{1}{2}}, t) - \boldsymbol{F}(x_{i-\frac{1}{2}}, t) \right] = 0. \tag{11.46}$$

3. Now, $\boldsymbol{F}(x_{i+\frac{1}{2}}, t)$ for $t > t_n$ is given by the solution of the Riemann problem with left state $\boldsymbol{U}_i^{(n)}$ and right state $\boldsymbol{U}_{i+1}^{(n)}$. At the interface, this solution is *independent* of time. We can hence write

$$\boldsymbol{F}(x_{i+\frac{1}{2}}, t) = \boldsymbol{F}^\star_{i+\frac{1}{2}}, \tag{11.47}$$

where $\boldsymbol{F}^\star_{i+\frac{1}{2}} = \boldsymbol{F}_{\text{Riemann}}(\boldsymbol{U}_i^{(n)}, \boldsymbol{U}_{i+1}^{(n)})$ is a short-hand notation for the corresponding Riemann solution sampled at the interface. Hence we now get

$$\Delta x \left[\boldsymbol{U}_i^{(n+1)} - \boldsymbol{U}_i^{(n)}\right] + \Delta t \left[\boldsymbol{F}^\star_{i+\frac{1}{2}} - \boldsymbol{F}^\star_{i-\frac{1}{2}}\right] = 0. \tag{11.48}$$

Or alternatively, as an explicit update formula:

$$\boldsymbol{U}_i^{(n+1)} = \boldsymbol{U}_i^{(n)} + \frac{\Delta t}{\Delta x}\left[\boldsymbol{F}^\star_{i-\frac{1}{2}} - \boldsymbol{F}^\star_{i+\frac{1}{2}}\right]. \tag{11.49}$$

The first term in the square bracket gives the flux that flows from left into the cell, the second term is the flux out of the cell on its right side. The idea to use the Riemann solution in the updating step is due to Godunov, that's why such schemes are often called *Godunov schemes*.

It is worthwhile to note that we haven't really made any approximation in the above (yet). In particular, if we calculate $\boldsymbol{F}_{\text{Riemann}}$ analytically (and hence exactly), then the above seems to account for the correct fluxes for arbitrarily long times. So does this mean that we get a perfectly accurate result even for very large timesteps? This certainly sounds too good to be true, so there must be a catch somewhere.

Indeed, there is. First of all, we have assumed that the Riemann problems are independent of each other and each describe infinite half-spaces. This is not true once we consider finite volume cells, but it is still OK for a while as long t_{n+1} is close enough to t_n such that the waves emanating in one interface have not yet arrived at the next interface left or right. This then leads to a CFL-timestep criterion, were $\Delta t \leq \Delta x / c_{\max}$ and $c_{\max}$ is the maximum wave speed.

Another point is more subtle and comes into play when we consider more than one timestep. We assumed that the $\boldsymbol{U}_i^{(n)}$ describe piece-wise constant states which can then be fed to the Riemann solver to give us the flux. However, even when this is true initially, we have just seen that after one timestep it will not be true anymore. By ignoring this in the subsequent timestep (which is done by performing an averaging step that washes out the cell substructure that developed as part of the evolution during the previous timestep) we make some error.

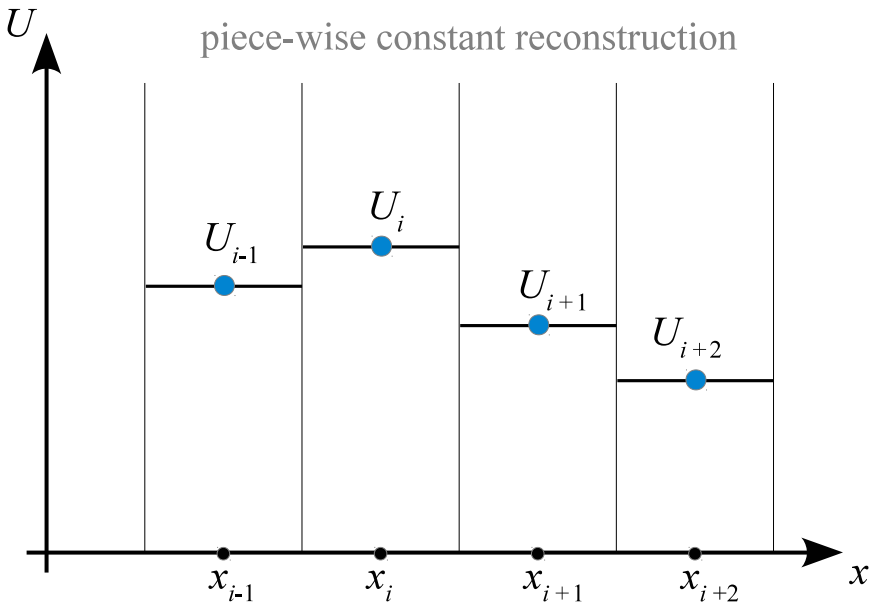

Figure 11.8: Piece-wise constant states of a fluid forming the simplest possible reconstruction of its state based on a set of discrete values U_i known at spatial positions x_i.

11.6 Godunov's method and Riemann solvers

It is useful to introduce another interpretation of common finite-volume discretizations of fluid dynamics, so-called Reconstruct-Evolve-Average (REA) schemes. We also use this here for a short summary of Godunov's important method, and the way Riemann solvers come into play in it.

An REA update scheme of a hydrodynamical system discretized on a mesh can be viewed as a sequence of three steps:

1. *Reconstruct:* Using the cell-averaged quantities (as shown in Fig. 11.8), this defines the run of these quantities everywhere in the cell. In the sketch, a piece-wise constant reconstruction is assumed, which is the simplest procedure one can use and leads to 1st order accuracy.

2. *Evolve:* The reconstructed state is then evolved forward in time by Δt. In Godunov's approach, this is done by treating each cell interface as a piece-wise constant initial value problem which is solved with the Riemann solver exactly or approximately. This solution is formally valid as long as the waves emanating from opposite sides of a cell do not yet start to interact. In practice, one therefore needs to limit the timestep Δt such that this does not happen.

3. *Average:* The wave structure resulting from the evolution over timestep Δt is

spatially averaged in a conservative fashion to compute new states $\boldsymbol{U}^{(n+1)}$ for each cell. Fortunately, the averaging step does not need to be done explicitly; instead it can simply be carried out by accounting for the fluxes that enter or leave the control volume of the cell. Then the whole cycle repeats again.

What is needed for the *evolve* step is a prescription to either exactly or approximately solve the Riemann problem for a piece-wise linear left and right state that are brought into contact at time $t = t_n$. Formally, this can be written as

$$\boldsymbol{F}^\star = \boldsymbol{F}_{\text{Riemann}}(\boldsymbol{U}_L, \boldsymbol{U}_R). \tag{11.50}$$

In practice, a variety of approximate Riemann solvers $\boldsymbol{F}_{\text{Riemann}}$ are commonly used in the literature (Rusanov, 1961; Harten et al., 1983; Toro, 1997; Miyoshi & Kusano, 2005). For the ideal gas and for isothermal gas, it is also possible to solve the Riemann problem exactly, but not in closed form (i.e. the solution involves an iterative root finding of a non-linear equation).

There are now two main issues left:

- How can this be extended to multiple spatial dimensions?
- How can it be extended such that a higher order integration accuracy both in space and time is reached?

We'll discuss these issues next.

11.7 Extensions to multiple dimensions

So far, we have considered *one-dimensional* hyperbolic conservation laws of the form

$$\partial_t \boldsymbol{U} + \partial_x \boldsymbol{F}(\boldsymbol{U}) = 0, \tag{11.51}$$

where ∂_t is a short-hand notation for $\partial_t = \frac{\partial}{\partial t}$, and similarly $\partial_x = \frac{\partial}{\partial x}$. For example, for isothermal gas with sound speed c_s, the state vector $\boldsymbol{U}$ and flux vector $\boldsymbol{F}(\boldsymbol{U})$ are given as

$$\boldsymbol{U} = \begin{pmatrix} \rho \\ \rho u \end{pmatrix}, \quad \boldsymbol{F} = \begin{pmatrix} \rho u \\ \rho u^2 + \rho c_s^2 \end{pmatrix}, \tag{11.52}$$

where u is the velocity in the x-direction.

In three dimensions, the PDEs describing a fluid become considerably more involved.

For example, the Euler equations for an ideal gas are given in explicit form as

$$\partial_t \begin{pmatrix} \rho \\ \rho u \\ \rho v \\ \rho w \\ \rho e \end{pmatrix} + \partial_x \begin{pmatrix} \rho u \\ \rho u^2 + P \\ \rho uv \\ \rho uw \\ \rho u(\rho e + P) \end{pmatrix} + \partial_y \begin{pmatrix} \rho v \\ \rho uv \\ \rho v^2 + P \\ \rho vw \\ \rho v(\rho e + P) \end{pmatrix} + \partial_z \begin{pmatrix} \rho w \\ \rho uw \\ \rho vw \\ \rho w^2 + P \\ \rho w(\rho e + P) \end{pmatrix} = \mathbf{0}, \tag{11.53}$$

where $e = e_{\rm th} + (u^2 + v^2 + w^2)/2$ is the total specific energy per unit mass, $e_{\rm th}$ is the thermal energy per unit mass, and $P = (\gamma - 1)\rho\, e_{\rm th}$ is the pressure. These equations are often written in the following notation:

$$\partial_t \boldsymbol{U} + \partial_x \boldsymbol{F} + \partial_y \boldsymbol{G} + \partial_z \boldsymbol{H} = \mathbf{0}. \tag{11.54}$$

Here the functions $\boldsymbol{F}(\boldsymbol{U})$, $\boldsymbol{G}(\boldsymbol{U})$, $\boldsymbol{H}(\boldsymbol{U})$ give the flux vectors in the x-, y- and z-direction, respectively.

11.7.1 Dimensional splitting

Let us now consider the three dimensionally split problems derived from equation (11.54):

$$\partial_t \boldsymbol{U} + \partial_x \boldsymbol{F} = \mathbf{0}, \tag{11.55}$$

$$\partial_t \boldsymbol{U} + \partial_y \boldsymbol{G} = \mathbf{0}, \tag{11.56}$$

$$\partial_t \boldsymbol{U} + \partial_z \boldsymbol{H} = \mathbf{0}. \tag{11.57}$$

Note that the vectors appearing here have still the same dimensionality as in the full equations. They are *augmented* one-dimensional problems, i.e. the transverse variables still appear but spatial differentiation happens only in one direction. Because of this, these additional transverse variables do not make the 1D problem more difficult compared to the 'pure' 1D problem considered earlier, but the fluxes appearing in them still need to be included.

Now let us assume that he have a method to solve/advance each of these one-dimensional problems. We can for example express this formally through time-evolution operators $\mathcal{X}(\Delta t)$, $\mathcal{Y}(\Delta t)$, and $\mathcal{Z}(\Delta t)$, which advance the solution by a timestep Δt. Then the full time advance of the system can for example be approximated by

$$\boldsymbol{U}^{(n+1)} \simeq \mathcal{Z}(\Delta t)\mathcal{Y}(\Delta t)\mathcal{X}(\Delta t)\boldsymbol{U}^{(n)}. \tag{11.58}$$

This is one possible dimensionally split update scheme. In fact, this is the exact solution if equations (11.55)-(11.57) represent the linear advection problem, but for more general

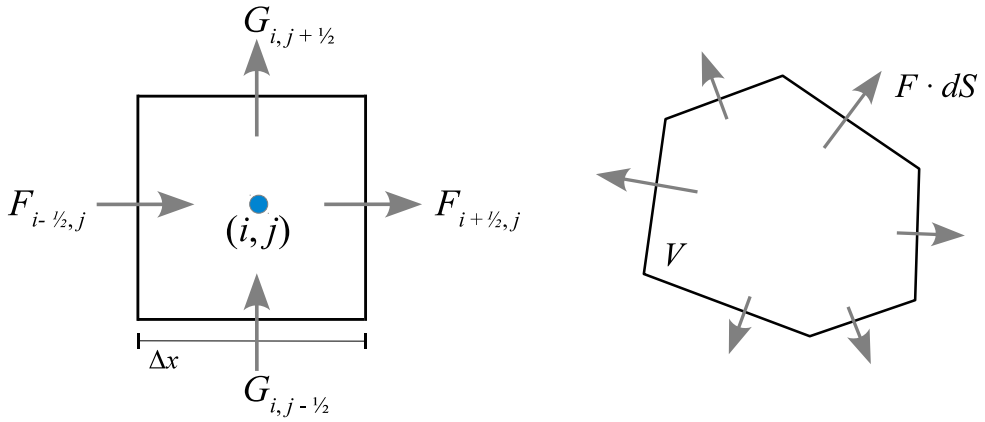

Figure 11.9: Sketch of unsplit finite-volume update schemes. On the left, the case of a structured Cartesian grid is shown, the case on the right is for an unstructured grid.

non-linear equations it only provides a first order approximation. However, higher-order dimensionally split update schemes can also be easily constructed. For example, in two-dimensions,

$$\boldsymbol{U}^{(n+1)} = \frac{1}{2}[\mathcal{X}(\Delta t)\mathcal{Y}(\Delta t)\mathcal{Z}(\Delta t) + \mathcal{Z}(\Delta t)\mathcal{Y}(\Delta t)\mathcal{X}(\Delta t)]\boldsymbol{U}^{(n)} \tag{11.59}$$

and

$$\boldsymbol{U}^{(n+1)} = \mathcal{X}(\Delta t/2)\mathcal{Y}(\Delta t/2)\mathcal{Z}(\Delta t)\mathcal{Y}(\Delta t/2)\mathcal{X}(\Delta t/2)\boldsymbol{U}^{(n)} \tag{11.60}$$

are second-order accurate. As a general rule of thumb, the time evolution operators have to be applied alternatingly in reverse order to reach second-order accuracy. We see that the dimensionless splitting reduces the problem effectively to a sequence of one-dimensional solution operations which are applied to multi-dimensional domains. Note that each one-dimensional operator leads to an update of $\boldsymbol{U}$, and is a complete step for the corresponding augmented one-dimensional problem. Gradients, etc., that are needed for the next step then have to be recomputed before the next time-evolution operator is applied. In practical applications of mesh codes, these one-dimensional solves are often called *sweeps*.

11.7.2 Unsplit schemes

In an unsplit approach, all flux updates of a cell are applied simultaneously to a cell, not sequentially. This is for example illustrated in 2D in the situations depicted in Figure 11.9. The unsplit update of cell i, j in the Cartesian case is then given by

$$\boldsymbol{U}_{i,j}^{(n+1)} = \boldsymbol{U}_{i,j}^{(n)} + \frac{\Delta t}{\Delta x}\left(\boldsymbol{F}_{i-\frac{1}{2},j} - \boldsymbol{F}_{i+\frac{1}{2},j}\right) + \frac{\Delta t}{\Delta y}\left(\boldsymbol{G}_{i,j-\frac{1}{2}} - \boldsymbol{G}_{i,j+\frac{1}{2}}\right). \tag{11.61}$$

Unsplit approaches can also be used for irregular shaped cells like those appearing in unstructured meshes (see Fig. 11.9). For example, integrating over a cell of volume V and denoting with $\boldsymbol{U}$ the cell average, we can write the cell update of equation (11.40) with the divergence theorem as

$$\boldsymbol{U}^{(n+1)} = \boldsymbol{U}^{(n)} - \frac{\Delta t}{V} \int \mathbf{F} \cdot d\boldsymbol{S}, \tag{11.62}$$

where the integration is over the whole cell surface, with outwards pointing face area vectors $d\boldsymbol{S}$.

11.8 Extensions for high-order accuracy

We should first clarify what we mean with higher order schemes. Loosely speaking, this refers to the convergence rate of a scheme in smooth regions of a flow. For example, if we know the analytic solution $\rho(x)$ for some problem, and then obtain a numerical result ρ_i at a set of N points at locations x_i, we can ask what the typical error of the solution is. One possibility to quantify this would be through a L1 error norm, for example in the form

$$L1 = \frac{1}{N} \sum_i |\rho_i - \rho(x_i)|, \tag{11.63}$$

which can be interpreted as the average error per cell. If we now measure this error quantitatively for different resolutions of the applied discretization, we would like to find that L1 decreases with increasing N. In such a case our numerical scheme is converging, and provided we use sufficient numerical resources, we have a chance to get below any desired absolute error level. But the *rate of convergence* can be very different between different numerical schemes when applied to the same problem. If a method shows a $L1 \propto N^{-1}$ scaling, it is said to be first-order accurate; a doubling of the number of cells will then cut the error in half. A second-order method has $L1 \propto N^{-2}$, meaning that a doubling of the number of cells can actually reduce the error by a factor of 4. This much better convergence rate is of course highly desirable. It is also possible to construct schemes with still higher convergence rates, but they tend to quickly become much more complex and computationally involved, so that one eventually reaches a point of diminishing return, depending on the specific type of problem. But the extra effort one needs to make to go from first to second-order is often very small, sometimes trivially small, so that one basically should always strive to try at least this.

A first step in constructing a 2nd order extension of Godunov's method is to replace the piece-wise constant with a piece-wise linear reconstruction. This requires that one first estimates gradients for each cell (usually by a simple finite difference formula). These are then slope-limited if needed such that the linear extrapolations of the cell states to the cell interfaces do not introduce new extrema. This slope-limiting procedure is quite

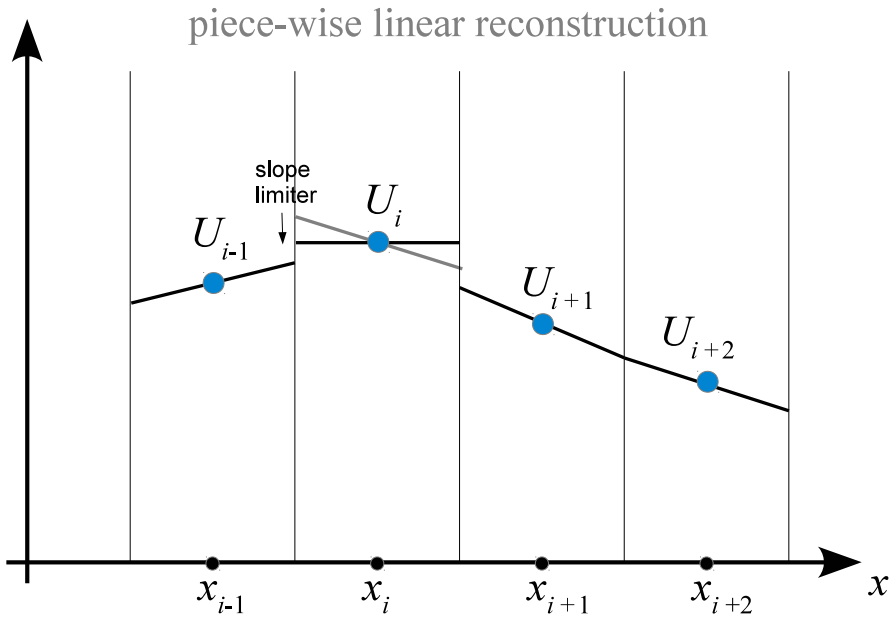

Figure 11.10: Piece-wise linear reconstruction scheme applied to a fluid state represented through a regular mesh.

important; it needs to be done to avoid that real fluid discontinuities introduce large spurious oscillations into the fluid.

Given slope limited gradients, for example $\boldsymbol{\nabla}\rho$ for the density, one can then estimate the left and right states adjacent to an interface $x_{i+\frac{1}{2}}$ by spatial extrapolation from the centers of the cells left and right from the interface:

$$\rho^L_{i+\frac{1}{2}} = \rho_i + (\boldsymbol{\nabla}_x \rho)_i \frac{\Delta x}{2}, \tag{11.64}$$

$$\rho^R_{i+\frac{1}{2}} = \rho_{i+1} - (\boldsymbol{\nabla}_x \rho)_{i+1} \frac{\Delta x}{2}. \tag{11.65}$$

The next step would in principle be to use these states in the Riemann solver. In doing this we will ignore the fact that our reconstruction has now a gradient over the cell; instead we still pretend that the fluid state can be taken as piece-wise constant left and right of the interface as far as the Riemann solver is concerned. However, our variables are functions of space and time so that a total differential obtains an additional contribution from varying the time:

$$\mathrm{d}\rho(r,t) = \frac{\partial \rho}{\partial x}\,\mathrm{d}x + \frac{\partial \rho}{\partial t}\,\mathrm{d}t. \tag{11.66}$$

This means that the spatial extrapolation needs to be augmented with a temporal extrapolation one half timestep into the future, such that the flux estimate is now effectively done in the middle of the timestep. This is necessary both to reach second-order

accuracy in time and also for stability reasons. Hence we really need to use

$$\rho^L_{i+\frac{1}{2}} = \rho_i + (\boldsymbol{\nabla}_x \rho)_i \frac{\Delta x}{2} + \left(\frac{\partial \rho}{\partial t}\right)_i \frac{\Delta t}{2}, \tag{11.67}$$

$$\rho^R_{i+\frac{1}{2}} = \rho_{i+1} - (\boldsymbol{\nabla}_x \rho)_{i+1} \frac{\Delta x}{2} + \left(\frac{\partial \rho}{\partial t}\right)_{i+1} \frac{\Delta t}{2}, \tag{11.68}$$

for extrapolating to the interfaces. More generally, this has to be done for the whole state vector of the system, i.e.,

$$\boldsymbol{U}^L_{i+\frac{1}{2}} = \boldsymbol{U}_i + (\partial_x \boldsymbol{U})_i \frac{\Delta x}{2} + (\partial_t \boldsymbol{U})_i \frac{\Delta t}{2}, \tag{11.69}$$

$$\boldsymbol{U}^R_{i+\frac{1}{2}} = \boldsymbol{U}_{i+1} - (\partial_x \boldsymbol{U})_{i+1} \frac{\Delta x}{2} + (\partial_t \boldsymbol{U})_{i+1} \frac{\Delta t}{2}. \tag{11.70}$$

Note that here the quantity $(\partial_x \boldsymbol{U})_i$ is a (slope-limited) *estimate* of the gradient in cell i, based on finite-differences plus a slope limiting procedure. Similarly, we somehow need to estimate the time derivative encoded in $(\partial_t \boldsymbol{U})_i$. How can this be done? One way to do this is to exploit the Jacobian matrix of the Euler equations. We can write the Euler equations as

$$\partial_t \boldsymbol{U} = -\partial_x \boldsymbol{F}(\boldsymbol{U}) = -\frac{\partial \boldsymbol{F}}{\partial \boldsymbol{U}} \cdot \partial_x \boldsymbol{U} = -\mathbf{A}(\boldsymbol{U}) \cdot \partial_x \boldsymbol{U}, \tag{11.71}$$

where $\mathbf{A}(\boldsymbol{U})$ is the Jacobian matrix. Using this, we can simply estimate the required time-derivative based on the spatial derivatives:

$$(\partial_t \boldsymbol{U})_i = -\mathbf{A}(\boldsymbol{U}_i) \cdot (\partial_x \boldsymbol{U})_i. \tag{11.72}$$

Hence the extrapolation can be done as

$$\boldsymbol{U}^L_{i+\frac{1}{2}} = \boldsymbol{U}_i + \left[\frac{\Delta x}{2}\mathbf{1} - \frac{\Delta t}{2}\mathbf{A}(\boldsymbol{U}_i)\right] \cdot (\partial_x \boldsymbol{U})_i, \tag{11.73}$$

$$\boldsymbol{U}^R_{i+\frac{1}{2}} = \boldsymbol{U}_{i+1} + \left[-\frac{\Delta x}{2}\mathbf{1} - \frac{\Delta t}{2}\mathbf{A}(\boldsymbol{U}_{i+1})\right] \cdot (\partial_x \boldsymbol{U})_{i+1}. \tag{11.74}$$

This procedure defines the so-called MUSCL-Hancock scheme (van Leer, 1984; Toro, 1997; van Leer, 2006), which is a 2nd-order accurate extension of Godunov's method.

Higher-order extensions such as the piece-wise parabolic method (PPM) start out with a higher order polynomial reconstruction. In the case of PPM, parabolic shapes are assumed in each cell instead of piece-wise linear states. The reconstruction is still guaranteed to be conservative, i.e. the integral underneath the reconstruction recovers the total values of the conserved variables individually in each cell. So-called ENO and WENO schemes (e.g. Balsara et al., 2009) use yet higher-order polynomials to reconstruct the state in a conservative fashion. Here many more cells in the environment need to be considered (i.e. the so-called *stencil* of these methods is much larger) to robustly determine the coefficients of the reconstruction. This can for example involve a least-square fitting procedure (Ollivier-Gooch, 1997).

References

Balsara, D. S., Rumpf, T., Dumbser, M., Munz, C.-D. (2009), *Efficient, high accuracy ADER-WENO schemes for hydrodynamics and divergence-free magnetohydrodynamics*, Journal of Computational Physics, 228, 2480

Courant, R., Friedrichs, K., Lewy, H. (1928), *Über die partiellen Differenzengleichungen der mathematischen Physik*, Mathematische Annalen, 100, 32

Field, G. B. (1965), *Thermal Instability.*, ApJ, 142, 531

Harten, A., Lax, P. D., Van Leer, B. (1983), *On upstream differencing and Godunov-type schemes for hyperbolic conservation laws*, SIAM Review, 25, 35

Kolmogorov, A. N. (1941), *Dissipation of Energy in the Locally Isotropic Turbulence*, Proceedings of the USSR Academy of Sciences, 32, 16

Landau, L. D., Lifshitz, E. M. (1959), *Fluid mechanics*, Course of theoretical physics, Oxford: Pergamon Press

LeVeque, R. J. (2002), *Finite volume methods for hyperbolic systems*, Cambridge University Press

Miyoshi, T., Kusano, K. (2005), *A multi-state HLL approximate Riemann solver for ideal magnetohydrodynamics*, Journal of Computational Physics, 208, 315

Mo, H., van den Bosch, F. C., White, S. (2010), *Galaxy Formation and Evolution*, Cambridge University Press

Ollivier-Gooch, C. F. (1997), *Quasi-ENO Schemes for Unstructured Meshes Based on Unlimited Data-Dependent Least-Squares Reconstruction*, Journal of Computational Physics, 133, 6

Pope, S. B. (2000), *Turbulent Flows*, Cambridge University Press

Pringle, J. E., King, A. (2007), *Astrophysical Flows*, Cambridge University Press

Rusanov, V. V. (1961), *Calculation of interaction of non-steady shock waves with obstacles*, J. Comput. Math. Phys. USSR, 1, 267

Shu, F. H. (1992), *The physics of astrophysics. Volume II: Gas dynamics.*, University Science Books, Mill Valley, CA

Stone, J. M., Gardiner, T. A., Teuben, P., Hawley, J. F., Simon, J. B. (2008), *Athena: A New Code for Astrophysical MHD*, ApJS, 178, 137

Toro, E. (1997), *Riemann solvers and numerical methods for fluid dynamics*, Springer

van Leer, B. (1984), *On the Relation Between the Upwind-Differencing Schemes of Godunov, Enguist, Osher and Roe*, SIAM J. Sci. Stat. Comput., 5, 1

van Leer, B. (2006), *Upwind and High-Resolution Methods for Compressible Flow: From Donor Cell to Residual-Distribution Schemes*, Communications in Computational Physics, 1, 192